Review

Review on Electrode Degradation at Fast Charging of Li-Ion and Li Metal Batteries from a Kinetic Perspective

Jinghui Miao

Lam Research Corporation, Fremont, CA 94538, USA; jinghui@alum.mit.edu

Abstract: With the surge of electric vehicles, fast charging has become one of the major challenges for the development of Li-ion and Li metal batteries. The degradation of battery electrodes at fast charging has been identified as among the gating factors. While there have been extensive studies on anode and cathode degradation modes, not sufficient efforts have been made to dive deep into the kinetics of battery charging and its influence on electrode degradation, especially during fast charging. This review presents a comprehensive yet concentrated perspective into such issues. By tracing back to the kinetic origins of battery charging, it is revealed that the intrinsic properties of electrode active materials and the microstructures of electrode are of great importance in determining electrode kinetics. Most of the electrode degradation modes are closely related to the high overpotentials and the spatial inhomogeneity in Li concentration and pertinent characteristics, which are results of the sluggish electrode kinetics during fast charging. Approaches to mitigate electrode degradation are summarized from the aspect of improving electrode kinetics and circumventing detrimental side reactions.

Keywords: Li-ion and Li metal batteries; fast charging; electrode kinetics; battery degradation

1. Introduction

In recent years, the "electrification of everything" has become a heated topic around the world. Lithium-based rechargeable batteries (Li-ion and Li metal batteries) have been extensively studied for their outstanding performance, namely higher energy density, higher power density, higher efficiency, and higher stability [1,2]. However, with the growing market of electric vehicles (EVs), one major obstacle has emerged for the development of lithium-based batteries, that is, whether they can withstand fast charging without sacrificing battery performance. Extreme fast charging (XFC) is defined as charging up to 80% of battery capacity within 15 min or less [3]. Currently, it is reported that Tesla's V3 supercharger offers a peak rate of 250 kW and can add up to 200 miles of range in 15 min [4,5]. Electrify America claims to offer charging speed as fast as 350 kW [6].

The risks of battery performance deterioration due to fast charging has been under the spotlight in the past few years, especially with the advancement in high-energy-density batteries. Prior work has demonstrated degrading battery performance, including worsening state-of-health (SoH) and coulombic efficiency (CE), as a result of fast charging [7,8]. The ability of Li-based batteries to keep up with fast charging is dependent on active material properties, cell design, and charging protocols. From a materials perspective, heterogeneous Li plating such as dendrite formation on the anode has been confirmed by experiments and simulations. It leads to the loss of Li inventory and destruction of battery structural integrity and hence results in capacity fade, short cycle life, short circuiting, and even thermally induced battery degradation in anodes such as Li metal and graphite [9–12]. Worse rate capability of Si thin film anode during full cell charging (anode lithiation) has been reported at 100 C charge rate as compared to during full cell discharging (anode delithiation), which is attributed to ohmic resistance and asymmetric voltage-concentration profiles [13]. Structural evolution in layered transition metal oxide cathodes, including

lattice distortion, phase transformation, and oxygen loss, along with the formation of cathode electrolyte interphase (CEI), all contribute to worse battery performance at normal rate over cycling [14–16]. Cathode degradation under fast charging conditions has not been extensively studied in the past, but the increased overpotential due to slow kinetics at high charge rate is expected to result in inhomogeneous charging and possibly overcharging parts of the active materials, which can worsen the structural integrity. In addition, increased lattice strain, cathode particle cracking, and surface reconstruction have been reported upon long cycling at high rate [17–20]. Aside from battery electrode materials, electrolyte, separator, and current collector design also play a role in battery fast charging. Temperature accelerates kinetic processes and is also of great importance [21].

Despite the growing attention to battery fast charging, there still remains a noticeable gap between the state-of-the-art technologies and the ultimate goals defined by XFC. This review is aimed to narrow this gap by examining the kinetically limiting processes of electrode reactions and underlying mechanisms of electrode degradation under fast charging, and providing insights into promising mitigation strategies on the cell level. In Section 2, the fundamentals of electrode kinetics and the rate-limiting steps in bulk electrodes and on electrolyte/electrode interfaces are reviewed, with the limitations of the simplified kinetic model addressed. The structural origins of the kinetically limiting processes are also discussed in example systems. In Section 3, a high-level summary of the impacts of fast charging is provided, followed by discussion of detailed electrode degradation mechanisms in anodes and cathodes. Finally, breakthroughs in alleviating electrode degradation under fast charging are highlighted in Section 4. Though not the focus of this review, it is also worth noting that significant efforts have been made beyond materials level and cell level to enable the commercialization of fast charging in Li-based batteries. This includes the optimization of charging protocols and thermal management systems, as well as the addition of safety devices and mechanical strategies to advance the overall performance reliability and longevity of Li-based batteries [22,23].

2. Battery Charging Kinetics

The literary work has unveiled that battery electrodes are in many cases the bottleneck of fast charging. This is because the processes taking place in electrodes are usually complicated in nature and kinetically slow under the operating conditions, while the ion conduction in liquid electrolyte is far more straightforward and orders of magnitude faster [24,25]. In this section, a simplified kinetic model for battery charging is presented, and the potential rate-limiting steps in cathodes and anodes are addressed, respectively.

2.1. A Simplified Kinetic Model of Battery Charging and Its Limitations

Battery charging process is often described in terms of two fluxes in opposite directions as compared to battery discharging process. One is the internal Li ion flux from the positive electrode through electrolyte to the negative electrode; the other is the external electron flux from the positive electrode through external electrical circuit to the negative electrode. When electrons are extracted from the positive electrode under external electric field, Li ions are dissolved in the electrolyte and migrate via ion conduction towards the negative electrode. They are accepted on the surface of the anode, and migrate into the bulk via solid-state diffusion under concentration gradient and electric field. Note that here electrodes are referred to as negative electrode (the electrode with lower potential, corresponding to the anode during full cell discharging) and positive electrode (the electrode with higher potential, corresponding to the cathode during full cell discharging). In all other sections of this review, they are referred to as anode and cathode as defined in full cell discharging, in order to ensure consistency in terminology with most publications in battery fast charging.

While this model incorporates the basic kinetic processes involved in battery charging and is hence informative, it does not sufficiently address some microscopic processes and has several limitations.

Firstly, electrodes are not always good electronic conductors. As shown in Section 2.2.1, most oxide-based cathodes are intrinsically semi-conducting or insulating. Some anode materials, such as non-doped Si, do not have high enough electronic conductivity either. It is therefore difficult to decouple ion transport under electric field from solid-state diffusion under concentration gradient in a simple manner.

Secondly, such a model fails to account for phase transformation in active materials. While many electrode reactions are limited by Li ion diffusion, the underlying mechanisms can be drastically different. Electrode lithiation and delithiation that involve phase transformation are more complex than those in single-phase systems (e.g., solid solution). Some phase-transforming electrode reactions are kinetically gated by the nucleation or growth of the new phase. Examples include the silicon, germanium, and aluminum anodes, in which one or multiple intermetallic phases are formed during lithiation [26–30].

Thirdly, driving forces for lithiation and delithiation in actual electrodes extend beyond the external electric field and the Li concentration gradient in electrodes. Researchers have reported noticeable electro-chemo-mechanical effects that develop large stress during some electrode reactions. The overpotential is controlled by multiple factors, making the kinetic picture of electrode charging less straightforward [31,32].

Fourthly, most electrodes under investigation are composite electrodes. The microstructure, including size and distribution of primary and secondary particles as well as electrode porosity and tortuosity, sometimes plays a more significant role in electrode kinetics. Such an impact should not be overlooked in the discussion of electrode reaction kinetics.

Lastly, the model does not take into consideration any side reaction at the electrode/electrolyte interface. SEI and CEI are observed in all types of Li-based batteries, which are closely related to the consumption of Li inventory and electrolyte and are believed to be major culprits for increased cell impedance. All of these may contribute to electrode degradation and definitely complicate electrode charging processes.

2.2. Rate-Limiting Steps in Electrode Charging from a Materials Perspective

Aside from the endeavors to improve battery protection devices and battery charging protocols, optimization of electrode materials is always among the most crucial solution to fast charging challenges. Due to the length of this review, this section only focuses on two primary sources that affect electrode kinetics: the intrinsic properties of electrode active materials and the electrode microstructures. Other factors, e.g., electrode design on a cell level, are also of great significance but are not covered here.

2.2.1. Intrinsic Properties of Electrode Active Materials

The selection of electrode active materials is the basis for electrode construction. Active materials may gate the charge rate by limiting electronic conduction, impeding mass transport, or by the sluggish phase transition kinetics, which not only affect the energy density and power density of batteries, but also contribute to electrode degradation at fast charging [33].

Electronic Conductivity The electronic conductivity of a material is intrinsically determined by its electronic band structure. Materials with Fermi level in the conduction band have sufficient electrons for transport and therefore high electronic conductivity. Such electrode materials include carbon-based anodes such as graphite, as well as metallic anodes such as Sn, Ge, and Li. On the other hand, some electrodes, such as $LiCoO_2$ (LCO) and $LiFePO_4$ (LFP) as cathode materials and $Li_4Ti_5O_{12}$ (LTO) and undoped Si as anode materials, have their Fermi level in the band gap. At room temperature, free charge carrier concentration in such materials is low and their electronic conductivity falls in the $10^{-4} \sim 10^{-9}$ S/cm range [34], compared to 10^4 S/cm for graphite [35]. However, their electronic conductivity can be improved by increasing the operating temperature and by increasing charge carrier density. While the former one is less controllable, it has been reported that the electronic conductivity of LFP is increased by Ru-doping [36], and the

electronic conductivity of LTO is also improved by F-doping [37]. Another factor that alters electronic conductivity in electrode is the state-of-charge (SoC). Young et al. reported that the electronic conductivity of LTO is increased by a factor of 10^6 at a partially lithiated state [38]. Pre-lithiation of LTO and partial cycling are thus recommended approaches to overcome the electronic conductivity barrier.

Li Ion Diffusivity Diffusion is essentially random jumps of the diffusing species to nearby lattice or interstitial sites. When migrating to other sites, Li ions need to overcome the potential posed by neighboring atoms, which are largely governed by the chemical environment and crystallographic characteristics of the electrode active material. Interstitial or lattice sites where lithium is strongly bound by its environment can lead to larger activation barriers for diffusion. The crystal structure of electrodes not only affects the diffusion barrier for Li ions, but also the concentration of available sites for random jumping [39]. In crystalline electrodes, Li diffusivity can differ significantly due to crystallographic anisotropy. For example, graphite is found to have much higher Li ion diffusivity ($\sim 10^{-7}$–10^{-6} cm^2/s) along the graphene planes with weak interatomic forces, compared to diffusion perpendicular to the graphene planes ($\sim 10^{-11}$ cm^2/s) [40]. In the case of LCO, Li ions prefer to occupy octahedral interstitial sites formed by close-packed oxygen. Experimental data show low diffusivity ranging from 10^{-11} to 10^{-12} cm^2/s when the (003) plane of LCO is perpendicular to Li flux [41,42]. In LFP, bulk Li diffusivity is very low ($\sim 10^{-14}$–10^{-16} cm^2/s) due to the fact that Li ions migrate via one-dimensional channel aligned with the [010] direction in the olivine structure [43]. Point defects along this migration path are likely to impede Li diffusion, unless nanosized LFP is used [44]. Examples of Li diffusion anisotropy are presented in Figure 1.
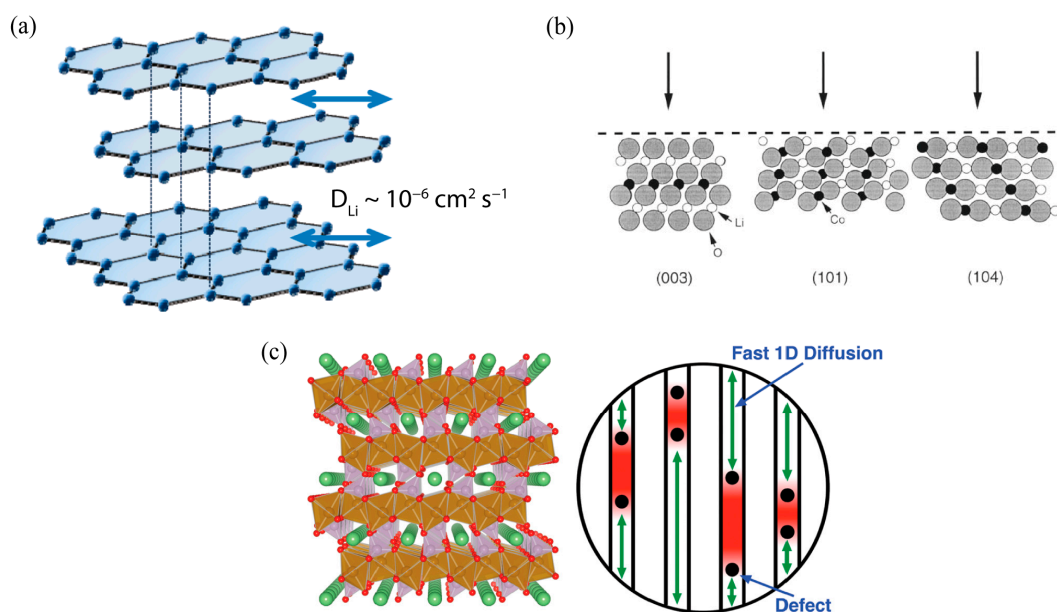

Figure 1. Anisotropy of Li ion diffusivity in crystalline electrodes: (**a**) graphite, reprinted with permission from [40], Copyright ©2010 American Chemical Society; (**b**) LCO, reprinted with permission from [41]; (**c**) LFP, reprinted with permission from [44], Copyright ©2010 American Chemical Society.

It is noteworthy that Li diffusivity is sensitive to lattice distortion caused by local Li concentration and the valence states of cations in the lattice (e.g., in transition metal oxide cathodes) [45]. There also exists strain-diffusion coupling in electrode materials (e.g., Si and Ge) that undergo large volumetric changes during cycling [46]. In addition, Li diffusion can occur via multiple pathways. Details are discussed in Section 2.2.2.

Phase Transition Kinetics As briefly addressed in Section 2.1, electrodes that are single-phase solid solution systems behave very differently compared to those with coexisting phases. When phase transitions in the electrodes are sluggish, mass transport may

no longer be the rate-limiting factor for charging. Phase transitions have been extensively studied in cathode materials [47–49] in the past. Recently, there have also been emerging interest in phase transitions in anode materials. Below, Figure 2 illustrates the correlations among phase transition, Gibbs free energy, and electrochemical potential during the lithiation of an example electrode (denoted as M).
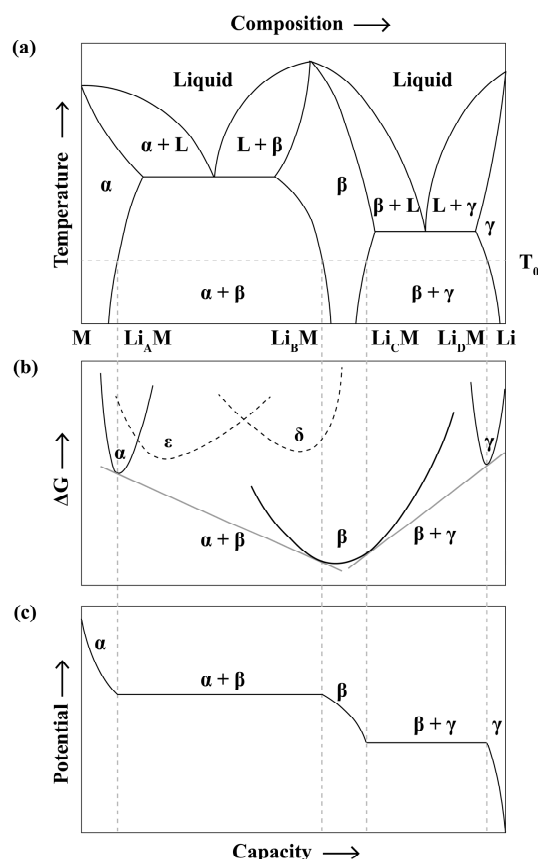

Figure 2. Schematics showing (**a**) the Li-M binary phase diagram, (**b**) Gibbs free energy as a function of Li composition at T_0, and (**c**) potential at T_0 as a function of Li composition. The stable intermediate phases are labelled as α, β, and γ, while unstable phases are labelled as ε and δ at T_0. Adapted with permission from [50].

Figure 2 depicts an example binary system between pure Li and an electrode material. With more Li inserted into the electrode, multiple phases are formed at T_0. The equilibrium phases are determined by the local minima of Gibbs free energy curve, subject to imposed constraints (e.g., temperature, pressure, etc.) The system remains a single phase in stoichiometric regimes corresponding to M->Li_AM, Li_BM->Li_CM, and Li_DM->Li. Two phases coexist in stoichiometric regimes where Gibbs free energy evolves along the common tangent line of two stable phases, corresponding to Li_AM->Li_BM and Li_CM->Li_DM.

According to the Gibbs phase rule (Equation (1)):

$$F = C - P + 2 \tag{1}$$

where C is the number of components, P is the number of coexisting phases, and F is the number of degrees of freedom. In a binary system where two phases coexist ($C = 2$, $P = 2$), the number of degrees of freedom equals to two, meaning there is no additional degree of freedom at fixed pressure and temperature. Therefore, potential (Figure 2c) remains constant when composition varies along the tangent line. In the single-phase regimes where solid solution composition varies with the degree of lithiation, there is an additional degree of freedom, leading to the negative slope in the potential vs. capacity plot.

Note that Figure 2 only applies to the systems that have first-order phase transitions (also referred to as discontinuous phase transitions). Such systems start with a metastable state and proceed with abrupt changes in order parameters, e.g., composition. Nucleation and growth of a new phase with a different structure or composition from the parent phase is a distinct feature of this type of phase transitions. Electrochemical evidence of first-order phase transitions includes a flat voltage plateau in the potential vs. capacity curve (as shown in Figure 2c), as well as a peak in the current transient under potentiostatic conditions [51,52]. Cathode materials such as LFP and $LiMn_2O_4$ (LMO) and anode materials such as Si and Ge fall into this category [30,51–53]. There are also systems where the phase transition proceeds by uphill diffusion from a thermodynamically unstable system without nucleation [54]. Such phase transitions are named spinodal decomposition or continuous phase transitions. Not many reports have focused on such systems, but Bai et al. proposed that LFP phase transition may also occur via spinodal decomposition based on simulation results [55].

Since nucleation and growth is a common pathway for phase transition in electrode materials, the nucleation barrier becomes a concern for fast charging. Recommendations to prevent the sluggish kinetics associated with nucleation and growth include (1) cycling electrode only in the solid solution regime [56], (2) circumventing nucleation by tuning the size of active materials and by optimizing charging protocols [55], and (3) minimizing nucleation barriers by minimizing the lattice misfits [52].

2.2.2. Microstructures of Electrodes

While the intrinsic characteristics of active materials provide sound explanations to some electrochemical behaviors, single-phase materials are rarely used as actual electrodes. This means that electrode kinetics, to a large extent, is affected or controlled by the microstructures of electrodes. A wide range of factors, including the crystallographic orientation of grains, the size distribution of grains or particles, and the porosity and tortuosity of particles, all need to be considered.

Grain Size and Crystallographic Orientation Grain size and crystallographic orientation in thin films and primary particles are closely related to electrode kinetics. When it comes to Li diffusivity, electrodes with smaller grains favor grain-boundary diffusion over in-grain diffusion as a result of smaller diffusion barrier [41,57,58]. In contrast, when average grain size is large and diffusion is dominantly in the bulk grains, there tends to be more variations in effective Li diffusivity due to crystallographic anisotropy. Numerical and experimental studies indicate that there is wide distribution of Li diffusivity in LCO cathodes with different grain sizes and orientations [41,57]. Experimental study indicates that single crystal LFP nanosheets with highly oriented (010) facets are promising high-rate cathode material [59]. Similarly, $LiNi_{0.8}Co_{0.1}Mn_{0.1}O_2$ (NCM811) also indicates that single-phase NCM811 outperforms small-grain NCM811 in terms of rate capability and capacity retention [60]. It is also found that single-crystal layered cathodes have better structural integrity and are less prone to cracking during battery cycling [61,62]. This gives them many advantages over small-grain polycrystalline electrode particles, including better rate capability. Note that the opposite may be true when there is large volumetric change in electrode during cycling, e.g., in single-crystal Si anodes [63].

While such impacts are most obvious in all-solid-state battery applications where thin film electrodes are most widely used [62], they have also been adopted in grain orientation and grain boundary engineering for electrode secondary particles to effectively improve electrode performance [64,65].

Particles Size, Electrode Porosity and Tortuosity Smaller particles are in general preferred for faster electrode kinetics. Larger and coarser particles are more prone to cracking and inhomogeneous lithiation, which is detrimental not only for fast charging but also for the overall lifespan of batteries [66]. Such a phenomenon is more notable in Si anodes, where the susceptibility of large particles to cracking is attributed to two major mechanisms: one is the larger concentration gradient during lithiation which is a

result of low Li diffusivity, and the other is the larger strain energy due to volumetric change [67]. Layered transition metal oxide cathodes have also been reported to have superior performance with smaller particles [68]. According to the percolation theory, larger spherical particles have relatively fewer contact points, resulting in fewer channels for electron conduction and ion diffusion [69]. In composite batteries, however, such disadvantage may be alleviated by independently manipulating the size of conductive additives. The worsened kinetic performance of electrodes with larger particles of active materials can also be explained by the accompanied longer transport ionic and electronic transport paths. In contrast, electrodes with smaller primary particles benefit from the large surface area and exhibit larger capacity at high charge rate [70]. For a solid electrolyte, active material particles with smaller grains can also better fill up the space and increase the volume utilization in electrodes [71]. However, when particles are very small, more SEI and CEI tend to form as a result of high surface area [66,72]. This introduces additional battery impedance which leads to battery degradation. A case-by-case analysis is often needed in composite electrodes, as the interplays between primary particles and secondary particles can be complicated in various electrode systems [72,73].

In addition to the average of particle size, particle size distribution in composite electrodes also plays an important role in determining electrode kinetics. Bläubaum et al. reported that graphite electrodes with a narrower distribution of particle size show better electrochemical performance [66]. Electrodes with wider distribution of particle size tend to behave like the larger particles, despite that the average particle size is smaller. At the same time, they are affected by multiple degradation mechanisms from smaller particles and from larger particles. Taleghani et al. developed a pseudo two-dimensional model and found that electrodes with mono-modal distribution of particle size have the most uniform local current density and thus the smallest polarization [74].

Electrode porosity and tortuosity are another two crucial parameters to describe the microstructure in composite electrodes. Composite electrodes are porous solid systems that consist of active material particles, additives, binders, and interconnected void space which is filled with liquid electrolyte. By definition, porosity is the percentage of the total volume of voids in the electrode. Tortuosity can be defined using the following equations:

$$D_{eff} = \frac{\epsilon}{\tau}D,$$ (2)

$$k_{eff} = \frac{\epsilon}{\tau}k_{int},$$ (3)

where ϵ is the porosity and τ is the tortuosity. D_{eff} and D are the effective and intrinsic diffusivities, and k_{eff} and k_{int} represent the effective and intrinsic conductivities. In other words, tortuosity measures the effective diffusion distance. Given a fixed porosity, structures with lower tortuosity have accelerated migration-related kinetics. Studies on LFP and graphite composite electrodes indicate that higher porosity leads to lower transport resistance, which in turn results in more homogeneous lithiation and better utilization of active electrode materials at higher charge rates [75,76]. It is further unveiled that pores small in size and isotropic in morphology contribute to lower tortuosity [76]. Controlling porosity and tortuosity by electrode engineering has become a heated topic under the development of fast charging. More examples are discussed in Section 4.

3. Electrode Degradation Mechanisms under Fast Charging

3.1. Effects of Fast Charging

Fast charging of EV batteries is achieved by specialized off-board chargers that can supply high currents. A conventional constant-current constant-voltage (CC-CV) charging scheme works by charging batteries first with a constant current until a preset voltage is reached and then maintaining a constant voltage until current drops below a threshold [77]. In order to charge faster, a higher current is used in the constant-current (CC) step of the protocol, which introduces additional risks to electrodes.

3.1.1. Overpotentials

When a battery is at its equilibrium potential, no flux flows in the system. Overpotential is indispensable in driving Li ion migration and subsequent reactions in a dynamic battery system. Below is a decomposition of electrode overpotential in a solid solution system [78]:

$$\Delta\varphi = \Delta\varphi_{AM} + \Delta\varphi_{CT} + \Delta\varphi_{EL}, \tag{4}$$

The total overpotential at each electrode ($\Delta\varphi$) is the sum of the overpotential for solid-state diffusion in the active material ($\Delta\varphi_{AM}$), the overpotential for electrode/electrolyte interface charge transfer ($\Delta\varphi_{CT}$), and the overpotential for ionic transport in electrolyte ($\Delta\varphi_{EL}$). The overpotentials associated with electrodes ($\Delta\varphi_{AM}$ and $\Delta\varphi_{CT}$) can be derived from the chemical potentials of Li ion at each electrode and are expressed as functions of charge current [78]:

$$\Delta\varphi_{AM} \propto I \cdot \frac{L}{A \cdot \widetilde{D}_{Li^+}}, \tag{5}$$

$$\Delta\varphi_{CT} \propto I \cdot \frac{1}{A \cdot j_0}, \tag{6}$$

where I is the charge current, A is the electrode surface area, L is the radius of active material particle, $\widetilde{D}_{Li^+}$ is the effective Li ion diffusivity, and j_0 is the exchange current density at the given electrolyte–electrode interface. It is obvious from Equations (5) and (6) that both overpotentials increase when charge current increases. Unfavorable parasitic reactions are therefore expected to occur at anode and/or cathode at elevated overpotentials. Two most widely studied examples are Li plating at the anode surface and transition metal oxide cathode decomposition (discussed in Sections 3.2 and 3.3).

In the case of phase-transforming electrodes (including intercalation-, alloying-, and conversion-type electrodes), it is believed that lithiation and delithiation proceed by phase boundary movement, rather than by a filling-up-the-tank model in single phase systems [26,28]. Chemical potentials across the phase boundaries are considered to be constant, and therefore there is no distinct current dependence of overpotentials in phase-transforming regimes. However, it is expected that concentration gradient exists within each phase and on the electrode level (see Section 3.1.2).

3.1.2. Spatial Inhomogeneity on the Electrode Level

In practice, high charge rate, coupled with sluggish Li ion diffusion in electrodes, often contributes to spatial inhomogeneity in Li concentration across electrodes.

On the anode side, operando energy dispersive X-ray diffraction (EDXRD) reveals that large Li concentration gradients exist from anode surface to bulk both in the Li-rich phase LiC_6 and Li-deficient phase $LiCl_{12}$ at 1 C charge rate in NCM/graphite coin cells [79]. A similar result is reported by Finegan et al. using high-speed depth-profiling synchrotron XRD that the average Li concentration in graphite anode drops significantly from anode surface to anode bulk close to the current collector at 6 C [80]. These all point to spatial variation of SoC during fast charging.

For cathodes, although little prior research has been conducted about the effect of fast charging on the spatial distribution of Li ions, significant degradation at 6 C charge rate has been observed in NCM/graphite batteries with higher cathode loading (2.5 mAh/cm^2 vs. 1.5 mAh/cm^2) [81], suggesting degradation mechanism(s) specific to thicker cathodes. In addition, Mistry et al. reported the effect of upstream perturbance from cathode on the spatial inhomogeneity in anodes. Localized Li ion flux from cathode may foster coincidental non-uniformity in Li intercalation and plating on the anode side [82].

To sum up, spatial inhomogeneity of Li concentration on the electrode level is a phenomenon closely related to fast charging, and hence is an important factor to consider when discussing electrode degradation mechanisms under fast charging. Such a spatial variation in concentration potentially results in spatial variation in overpotential (and therefore the

propensity to unfavored reactions), stress, and temperature. These are addressed in more detail in Sections 3.2.2 and 3.3.2.

3.2. Anode Degradation at Fast Charging

Fast charging has been believed by many to be an anode-centric issue. This is primarily because of the difficulty in ensuring uniform and reversible Li intercalation, reaction, and/or plating on the anode side.

3.2.1. Li Plating in Li-Ion Batteries and Li Metal Batteries

Li plating occurs in the fast charging of both Li-ion batteries and Li metal batteries. Its origin and effect on battery performance, however, differ in these two types of batteries.

In Li-ion batteries, reversible Li intercalation into the anode material is the dominant reaction and Li plating rarely occurs at low or moderate charge rate in the normal operating window. However, electrode polarization is increased at high charge rate due to relatively slow intercalation or electrode reaction, and results in larger overpotentials, making the anode (graphite in most cases) more prone to Li plating in parallel with intercalation [83]. From this perspective, the utilization of high-voltage anodes such as LTO and niobium-based oxide anodes (Nb_2O_5, $TiNb_2O_7$, etc.) can effectively prevent Li plating [84]. These anodes, however, suffer from other disadvantages such as low intrinsic electronic conductivity and hydrogen outgassing, which are also unfavorable for fast charging applications [85,86]. Figure 3 summarizes a few practical factors to consider for Li plating on graphite. Aside from the thermodynamic driving force from large electrode polarization (Figure 3a), Li plating could also be triggered if Li is saturated on the surface of anode due to slow solid-state diffusion versus intercalation. (Figure 3b). Once Li plating overcomes the nucleation barrier on graphite, the subsequent Li growth proceeds in a kinetically more favorable fashion.
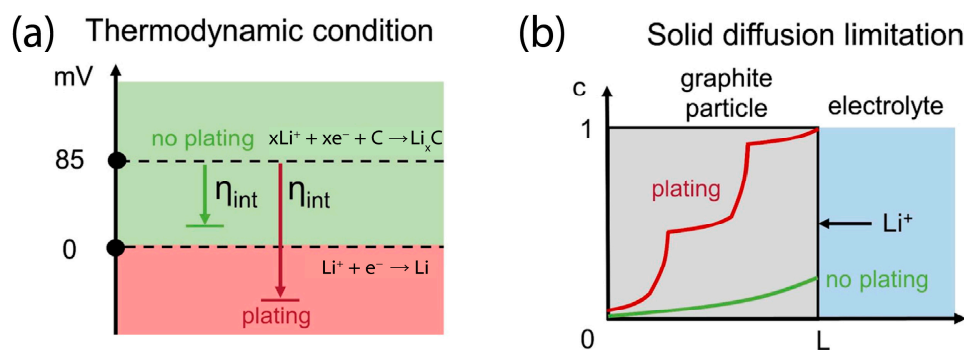

Figure 3. Mechanisms for Li plating on graphite, adapted with permission from [87]. Li plating can occur when (**a**) intercalation overpotential (η_{int}) is large enough to meet the thermodynamic criterion for Li plating (V < 0 versus Li/Li$^+$), or when (**b**) solid diffusion in the electrode is sluggish so that Li concentration is saturated at electrode surface.

In Li metal batteries, however, Li plating is a normal process occurring during charging. It is worth noting that Li plating itself is not necessarily detrimental to battery performance, but the heterogeneously plated Li in Li-ion batteries and Li metal batteries does introduce extra risks regarding battery performance and safety. Various morphologies of plated Li has been reported over the years, including dendrites [88], whiskers [89], and agglomerations [90] (Figure 4). Density functional theory (DFT) study substantiates the tendency of Li to form low-dimensional morphologies [91]. Sand's time has been adopted to estimate when uniform electrodeposition would transition into dendrite growth as a result of depleted cation concentration at electrode surface [92]. However, experimental evidence suggests much earlier commencement of Li dendrite growth than predicted by Equation (7). It is proposed that Li ion transport through SEI should be counted in a modified Sand's equation to better capture the onset of Li dendrite formation. It is also noteworthy that

the abovementioned model is based on a flat substrate. In reality, non-ideal anode surface characteristics also play a significant role in determining the onset of Li dendrite formation [93,94]. Surface modification and passivation layer have both been utilized for electrode engineering (see Section 4).
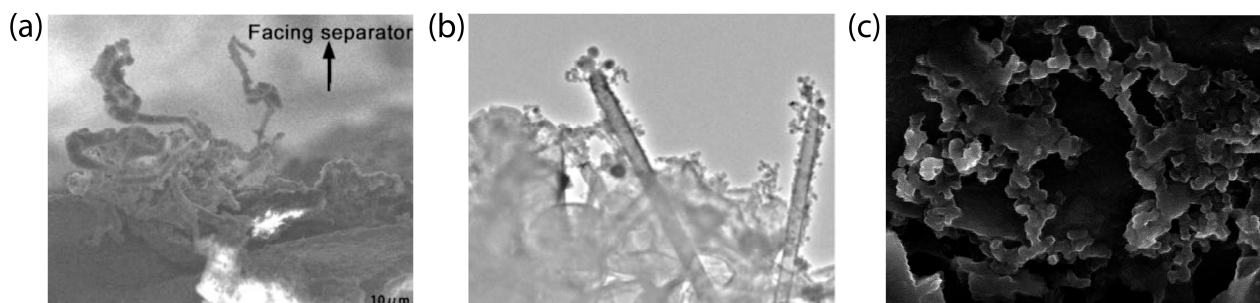

Figure 4. Typical morphologies of plated Li on anode surface: (**a**) dendrites, reprinted with permission from [88], © 2019 Elsevier; (**b**) whiskers, reprinted with permission from [89]; (**c**) agglomerations, reprinted with permission from [90].

In addition, the applied current density, anode microstructure, and electrolyte composition are all among the factors that affect the morphology of plated Li [95]. The poorly controlled Li microstructures then function as hotspots for preferential Li plating as a result of concentrated local current density, heat, and stress [96,97]. Heterogeneous Li plating is notorious for three main reasons. Firstly, continued Li plating and stripping inevitably consumes the Li inventory by creating "dead" Li and by side reactions with liquid electrolyte which consumes electrolyte as well [98]. Secondly, when dendritic structures are formed, the separator or the solid electrolyte layer may get damaged or even penetrated, increasing the risk of internal short circuiting and thermal runaway [99]. Thirdly, non-uniform and dynamic Li plating destroys the integrity of anode/electrolyte interface [100]. The growing SEI greatly increases interfacial resistance over cycling and thus further promotes heterogeneous Li plating.

3.2.2. Anode Degradation Modes Aggravated by Fast Charging

Different from Li plating, which rarely occurs at slow charge rate, there are some other anode degradation modes which exist at all charge rates. It is still worthwhile to briefly review their origins and adverse impacts on electrodes because the spatial inhomogeneity in Li concentration (discussed in Section 3.1.2) tends to aggravate such degradation modes at fast charge rate. This section covers two most common anode degradation mechanisms: unstable SEI formation and mechanical degradation.

SEI is the product of electrode–electrolyte side reactions and exists in liquid-electrolyte-based batteries and solid-state batteries. Figure 5a explains the origin for SEI formation and Figure 5b is an image showing SEI on active material surface. Φ_C and Φ_A stand for work functions for cathode and anode, the difference of which is the battery voltage, V_{cell}. The electrolyte is stable when the chemical potentials of anode and cathode (μ_A and μ_C, respectively) fall between its lowest unoccupied molecular orbital (LUMO) and highest occupied molecular orbital (HOMO). Beyond the scope, SEI is formed to passivate the electrodes. In most of the literature, only the passivation layer at anode/electrolyte interface is named SEI, while the passivation layer at cathode/electrolyte interface is called CEI (cathode electrolyte interphase). They are essentially layers of electrolyte decomposition products, obtained either by electrolyte reduction at the anode material surface or by electrolyte oxidation at the cathode material surface.
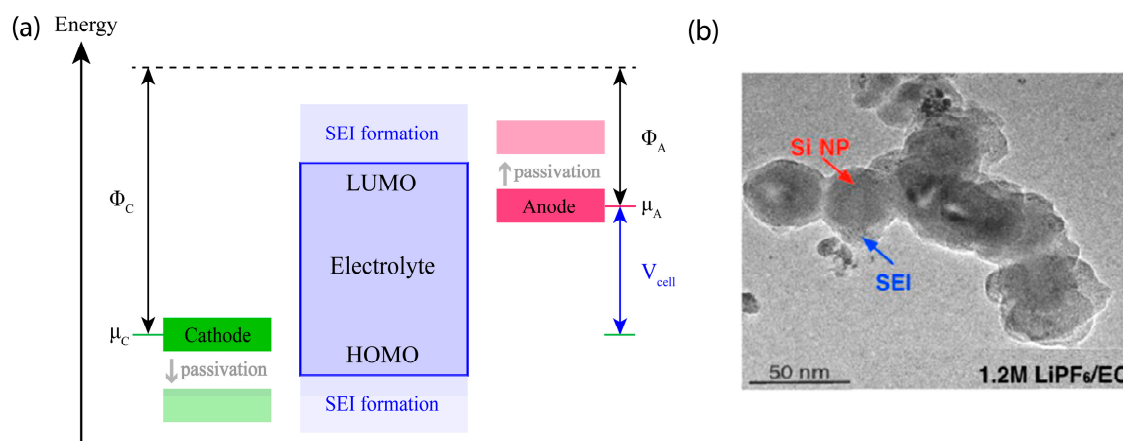
Figure 5. (**a**) Schematic of the stable voltage window of a liquid electrolyte; (**b**) Transmission electron microscopic (TEM) image showing SEI layer on the surface of Si nanoparticles (NP), reprinted with permission [101], Copyright © 2013 American Chemical Society.

SEI growth is self-limiting and can form a passivation layer which stops electrolyte consumption and Li inventory loss [102]. In addition, SEI helps to reduce interfacial resistance in solid state batteries where the contact between solid electrolyte and solid electrodes is poor [103]. However, SEI failure can happen thermally, chemically, and mechanically. Thermal decomposition of SEI occurs at elevated temperature. In the case of fast charging, there is a risk of temperature increase when the generated heat cannot be timely dissipated [104]. Chemical failure involves the continuing reaction between SEI and electrolyte over elongated cycling [105]. Mechanical failure refers to the destruction of a continuous SEI layer when anode is under cyclic tensile and compressive stress during cycling. This is most commonly seen in Si-based anodes [106] and Li metal anodes [107]. When fresh anode surfaces are exposed, more side reactions ensue, which further consumes active material and electrolyte and acts as an additional kinetic barrier in fast charging.

Mechanical degradation is also common in anode active materials, as they suffer from cyclic stress during cycling. The mechanical failure mechanism for Li metal anodes is closely related to the non-uniform Li plating, which has been discussed in Section 3.2.1. Another example is Si-based anodes. As Si forms a series of Li-rich alloy phases during lithiation, its structure is altered significantly to accommodate the large amounts of Li. As a result, strain energy accumulates and eventually strain energy is released in the form of mechanical failure. Figure 6 illustrates some characteristic cracking patterns observed in Si-based anodes. In single crystal Si wafers, variations in crack orientation suggest the strong anisotropy in Li diffusion and elastic moduli (Figure 6a) [108]. In amorphous Si thin film anodes, crack formation is usually randomly oriented (Figure 6b) [109]. Figure 6c exhibits the morphological evolution of a patterned film, where a dome-shaped feature is formed as there is less constraint near the top of the film [110]. The morphological changes in Si nanoparticles and Si nanowires are more isotropic (Figure 6d,e) [111,112]. Despite the difference in structures, all Si-based anodes exhibit size-dependent crack/facture characteristics. Si active materials remain intact below a critical size [112–114], which is sensitive to factors such as electrode structure, fabrication method, and cycling protocol.
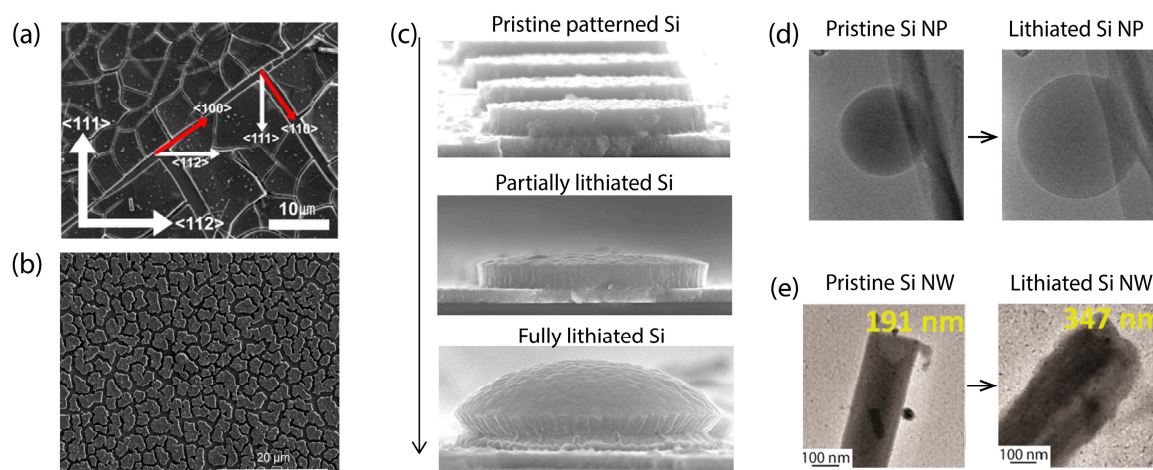
Figure 6. Scanning electron microscopy (SEM) and TEM images showing structural changes in lithiated Si anodes: (**a**) single crystal Si wafer, reprinted with permission from [108], Copyright © 2014 Elsevier; (**b**) thin film Si, reprinted with permission from [109]; (**c**) patterned Si film, adapted with permission from [110], Copyright © 2013 American Chemical Society; (**d**) Si nanoparticle (NP), adapted with permission from [111], Copyright © 2013 American Chemical Society; (**e**) Si nanowire (NW), adapted with permission from [113].

There have been inconsistent conclusions about the sensitivity of mechanical degradation to charge rate in alloying anodes. Liu et al. claimed that lithiation-induced stress in Si particles dominantly occurs at the phase boundary and is independent of charge rate as in single-phase regimes [112]. In contrary, Barai et al. reported enhanced mechanical degradation at higher lithiation rates in Sn particles, as strain energy relaxation by creeping is not dominating at high rate [115]. These conflicting observations point to the complex and multi-scale nature of mechanical degradation processes. It is also worth noting that fast charging induces a Li concentration gradient on the electrode level, which further induces spatial inhomogeneity in stress distribution even in materials that undergo phase transitions. While a sharp interface is observed in Si anodes in the initial lithiation, no such interface is observable in subsequent cycles. However, nuclear magnetic resonance (NMR) and pair distribution function (PDF) analysis have reported the existence and evolution of short- and medium-range orders in the lithiation of Si and Ge beyond the first cycle [116–121], suggesting such anodes experience reversible phase transitions between metastable phases. Potentiostatic experiments have also revealed non-monotonical current transients, which are indicative of the nucleation and growth processes in such systems, even when a sharp phase boundary is absent [30,51]. Though there has not been systematic study on the effect of charge rate on phase-transition induced stress where no sharp phase boundary is observed, distinction should be made considering the drastically different characteristics of phases transitions, and the charge-rate dependence should be discussed separately.

3.3. Cathode Degradation at Fast Charging

Compared to anode materials, cathode materials have lower specific capacity and in general slower electrode kinetics, rendering them more and more of a bottleneck for battery performance improvement [122]. Although most research has focused on anode degradation mechanisms under fast charging, cathode material is indeed of great importance in ensuring reasonable battery performance. For example, Chinnam et al. unveiled that cathode degradation due to loss of active material is the leading cause of aging in low-loading graphite/NMC532 single-layer pouch cells, while anode degradation due to Li plating is the dominant mechanism in moderate-loading cells [123]. In high loading cells, it has also been reported that cathode material properties play a crucial role in battery capacity retention at high charge rate [8].

3.3.1. Cathode Instability and Decomposition at High Overpotential

Despite limited research on fast charging kinetics on cathode materials, it is not hard to deduce that cathode materials are more susceptible to intrinsic structural instabilities at high charge rate due to elevated overpotential [16]. In this section, the focus will be on structure-specific degradation mechanisms at high overpotentials. The example systems covered are LCO, $LiNi_xCo_yMn_{1-x-y}O_2$ (NCM or NMC), $LiNi_xCo_yAl_{1-x-y}O_2$ (NCA), LFP, and LMO.

LCO LCO has been the most widely used commercial battery cathode for more than two decades [124]. While it has a theoretical capacity of 274 mAh/g, only about 140 mAh/g can be utilized in commercial batteries due to constraint of the operating voltage [125]. When charged over 4.35 V, a large amount of Li is extracted, and the layered structure undergoes irreversible transition from the hexagonal phase H3 to the hybridized H1–3 phase and the O1 phase [126]. TEM study has suggested that HT-LCO transforms to a spinel structure upon cycling [127]. The instability of these transitions and the resulting phases lead to tremendous deterioration in battery performance. On the other hand, LCO performance also degrades with cycling. The side reactions at the LCO/electrolyte interface are the major culprits of cell impedance rise and battery aging [128].

Moving Towards Co-free Cathodes There has been increasing concern about the economic, security, and societal impacts of LCO on EV applications, which would require massive amounts of Co [129]. As a result, the focus of cathode material research has been shifting to developing cathodes that have less Co content or completely Co-free while still possessing high capacity.

One type of such cathodes is layered transition metal oxide cathodes, in which Co is partially substituted with other metallic elements (e.g., Ni, Mn, and Al). Examples of this family include cathodes with lower Ni content such as $LiNi_{1/3}Co_{1/3}Mn_{1/3}O_2$ (NCM111), and Ni-rich cathodes such as $LiNi_{0.8}Co_{0.1}Mn_{0.1}O_2$ (NCM811) and $LiNi_{0.85}Co_{0.1}Al_{0.05}O_2$ (NCA8515). Ni-rich layered transition oxide cathodes have some shared challenges. Firstly, while the specific capacity of cathode increases with higher Ni content, the crystal structural instability and the extent of cation mixing is also increased at deep delithiation, which is a concern for fast charging applications. Ni cations tend to migrate to octahedral site in the Li layer and lead to undesirable layered-spinel-rock salt phase transitions when delithiated [130–132]. Secondly, the reduction of Ni^{4+} to Ni^{2+} is accompanied by the release of oxygen and heat. The generated oxygen vacancies accelerate Ni migration and facilitate more oxygen release, which significantly increases the likelihood of side reactions with electrolyte and catastrophic thermal runaway [133]. Thirdly, the excess Li ions on the surface of Ni-rich cathodes tend to react with air and accelerate metal dissolution, which both lead to capacity decay [134]. Released oxygen can continue to form surface layers on the cathode which impede charge transfer [135]. It is reported that NCA8515 has better capacity retention and cycling stability over NCM811 in spite of higher Ni content. The reason is that Mn dissolution results in Ni dissolution, which also exacerbates cation mixing between Li and Ni [136]. It is also worth noting that although higher Al content in NCA helps with structural stabilization, it is harmful for cell impedance [137]. In contrast, NCM111 has relatively lower capacity, but much better structural stability compared to Ni-rich counterparts [138]. Figure 7 is a schematic visualization of the abovementioned cathode crystal structures and the Ni/Li cation mixing process. For NCM cathodes, Yang et al. reported significant impact of fast charging at 6 C on overpotential, SOC, and capacity retention over cycling, especially on high loading cathodes where capacity is reduced by more than 20% in less than five cycles [8].
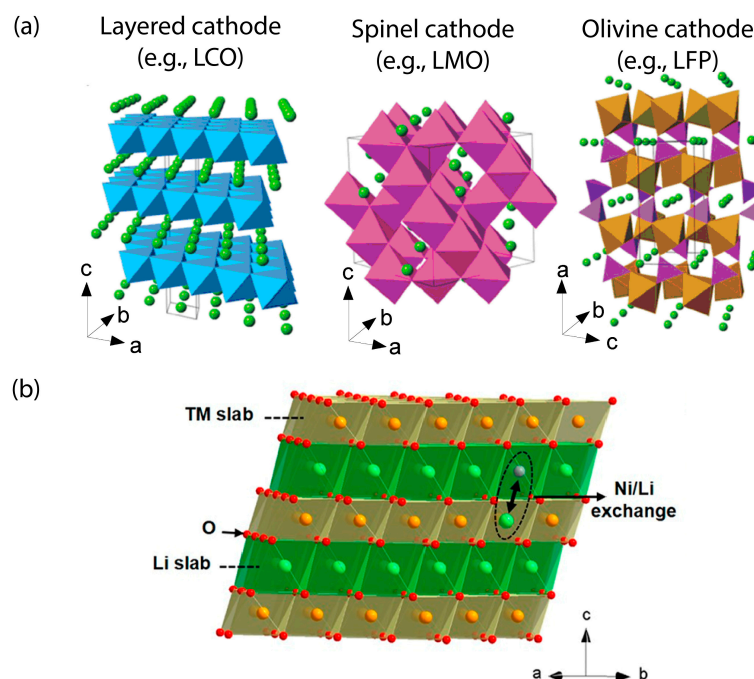
Figure 7. Schematics of crystal structures of (**a**) layered, spinel, and olivine structured cathodes, adapted with permission from [139]; (**b**) cation mixing of Ni and Li in Ni-rich transition metal oxide cathodes, reprinted with permission from [130], Copyright © 2019 American Chemical Society.

Another promising cathode, LMO, adopts a spinel structure. LMO degradation has been attributed primarily to structural instability at deep delithiated state, which is again a concern for fast charging applications. LMO undergoes the $Mn^{3.5+}/Mn^{4+}$ redox reaction at approximately 4 V, and then transforms into the over-delithiated phase Li_2MnO_4 at 3 V. Accompanying this phase transition is an anisotropic volume change (Jan–Teller distortion) and the resulting local mechanical strain [140]. Although delithiation to Li_2MnO_4 contributes to a high capacity of around 285 mAh/g, acceleration of capacity decay has been observed simultaneously [141].

3.3.2. Cathode Degradation Modes Aggravated by Fast Charging

Some types of cathode degradation, such as mechanical failure, CEI formation, and metal dissolution, are not unique to fast charging scenarios rate [142–144]. Not enough research has been conducted and their dependence on charge rate remains elusive. Woodford et al. simulated stress distribution in LMO particles and discovered that coherency stress is dominant in phase-transition regimes, which is independent of charge rate [145,146]. However, Xu et al. demonstrated that mechanical degradation in NMC composite cathodes is a function of lithiation state and that the microscopic heterogeneity in composite electrodes may render different behaviors [147]. As discussed in Section 2.2.2, fast charging may accelerate undesirable processes in cathodes depending on the microstructure of electrodes. In some cases, electrode engineering aimed to improve the rate capability of cathodes can introduce additional degradation pathways. One example is the adoption of carbon black (CB) in LFP, which has low electronic conductivity and Li ion diffusivity [148]. LFP composite electrodes can degrade by CB agglomeration and loss of crystallinity [149] over elongated cycling. NMC particles have also been found to detach from carbon/binder domain more seriously under higher charge rate, again alluding to the fact that fast charging has adverse effects on various electrode components [150].

4. Solutions to Electrode Degradation for Fast Charging Applications

There are two categories of mitigation strategies to confront battery failure. The first is to reduce the risk of various failure modes during normal operation, and the other is to evade or contain disasters in the event of failure [151]. This section focuses on the first category, which emphasizes on improving the intrinsic performance of batteries via electrode engineering. It should be noted that there are always tradeoffs between battery characteristics, e.g., improving rate capability at the expense of lowering specific capacity and energy density. Often times, multiple approaches are required to reach optimal battery performance.

4.1. Composition Optimization

Composition optimization can be achieved by tuning existing chemistry of electrode active materials, or by changing the component phases in composite electrodes.

On the anode side, doping and alloying have been proved effective to improve higher capacity and rate capability. To utilize the high capacity of Si anodes, boron doping is implemented, which increases the electronic conductivity and Li diffusivity in Si films [152]. Ge has also been used as dopant in LTO, leading to reduced particle size and increased electronic conductivity that contribute to much-improved capacity, rate capability, and cycling stability [153]. A hybrid anode synthesized by uniformly implanted amorphous Si nanolayer and graphite is reported with exceptional fast-charging behavior [154]. On the cathode side, composition tuning has achieved impressive progress in layered transition metal oxide cathodes. As is covered in Section 3.3.1., higher Ni content leads to higher capacity and energy density, but increases the risk of cathode collapse and oxygen release [132]. Mn and Al are relatively stable and thus used as structure stabilizer, while Co is reportedly beneficial in postponing Ni-dominated cathode degradation [155]. To avoid mechanical degradation induced by phase transition in spinel structures, Fe-doping is proposed to extend the solubility of Li over the composition window of cathode lithiation and delithiation [145]. Such an approach mitigates the risk of charge rate dependent fracture even at large particle size.

A common and feasible approach to speed up electrode kinetics is by forming composite electrodes with conductive additives. Carbon black has been used for a long time to improve the electronic conductivity in composite electrodes. There has been progress both in using conductive matrix including carbon fibers and carbon nanotubes [156,157] and in adding conductive materials to the matrix of active materials (e.g., LTO) [158] for better electron conduction and Li diffusion. Binder optimization is also of great importance to ensure robust, low-resistance, and continuous internal pathways in composite electrodes. For conventional nonconductive binders, polymers containing carboxylic groups such as alginate have been used to protect electrodes with substantial volume change by forming a passivation layer [159]. Conductive binders, on the other hand, are multifunctioning in that they provide structural support along with electron transport pathways. Efforts have been made to tailor the molecular structure as well as 3D microstructures [160].

4.2. Surface Modification

Surface modification is one of the most widely adopted approaches for electrode engineering. It can benefit fast charging and circumvent electrode degradation by passivating electrode surface, improving homogeneity of surface reactions, and increasing interfacial contact for faster kinetics. Some examples are illustrated in Figure 8.
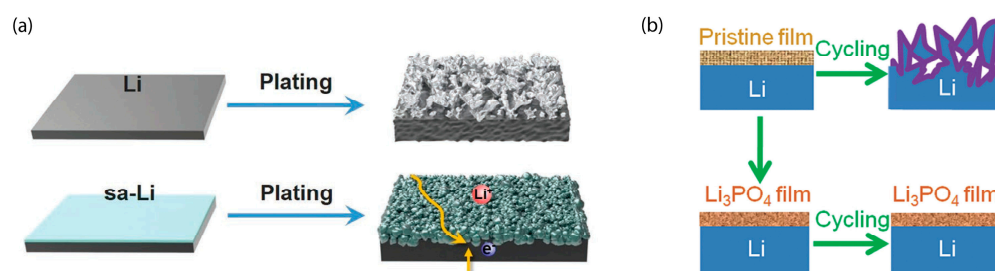
Figure 8. Schematics showing two types of surface modification techniques: (**a**) by surface alloying, reprinted with permission from [161]; (**b**) by artificial SEI layer, reprinted with permission from [162].

Artificial passivation layers are usually electronic insulators and ionic conductors. They are resistant to electrolyte corrosion and are mechanically robust. For instance, a ZrO_2 coating has been applied to Ni-rich cathodes to suppress metal dissolution and improve electrode kinetics [163]. Surface alloying by laminating Si with Li metal creates a rigid Li–Si alloy, and surface passivation by a thin SiO_2 layer both prevent non-uniform Li plating during fast charging [161,164]. Li_3PO_4 and LiPON have also been reported as a protective layer to stabilize Si anodes from cracking and pulverization and to stop further reaction with electrolyte during cycling [162,165,166].

Surface modifications also help by mitigating non-uniform surface reactions on electrodes. Different coatings, including Au [167,168], ZnO/carbon nanotube [169], and Li-Sn alloy [170], have been utilized to guide Li plating and prevent detrimental dendrite growth.

Poor interfacial contact and high interfacial impedance have been primary challenges for fast charging using solid state Li metal batteries. Efforts have been made to improve the wettability of Li by coating garnet-type solid electrolyte with SnS_2 nanosheet [171] and AlN layer [172], which either has high affinity to Li or forms intermetallic compounds with Li.

4.3. Microstructure Control

Electrode microstructure is key to conduction and diffusion kinetics, as well as to structural and mechanical stability. A good balance is needed between achieving good electrode kinetics and maintaining high enough capacity.

In composite electrodes, it is known that higher porosity combined with lower tortuosity is beneficial for faster kinetics, especially for thick electrodes. KOH-etched graphite anode is a good example which shows improved rate capability and cyclability as a result of increased porosity [173]. With a fixed porosity, aligned structures tend to have lower tortuosity as Li diffusion distance is shortened [174]. Chen et al. fabricated a highly ordered laser-patterned graphite electrode. With the highly aligned holes connecting electrolyte and the current collector, the high-rate performance is significantly improved [175]. Zhao et al. constructed a vertically channeled sandwich structure, with LFP nanoparticles entrapped in the graphene wall [176]. Such a structure not only exhibits impressive rate capability but also great structural integrity. Moreover, Yang et al. designed a porosity gradient graphite anode, with the largest porosity near anode surface and the smallest porosity near the current collector [177]. Compared with graphite anode with uniform bulk porosity, the new design effectively increases the transport rate near anode surface and alleviates Li plating on the anode surface. Scaffold structures are another scheme to guide Li plating inside the porous anode, which prevents surface plating and potential dendrite growth [178].

For Si-based and Ge-based anodes, their microstructure also plays a crucial role in retaining cycling performance. As discussed in Section 3.2.2, the colossal volume change of alloying anodes is a bottleneck in many applications. Nanostructured anodes, including nanowires [179], nanotubes [180], and nanoparticles [181], have been used to accommodate the volume expansion during lithiation. More complicated 3D architectures, such as honeycomb-like structures [182], core-shell structures [183,184], and multilayers [185], have also been designed to further buffer the volume expansion. Figure 9 summarizes some progress in microstructure control for better electrode kinetics.
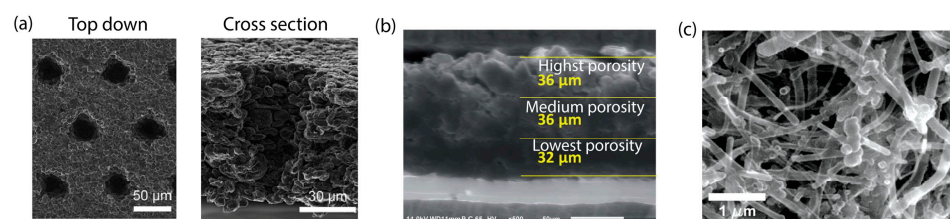
Figure 9. SEM and TEM images of (**a**) highly aligned holes in graphite anode, reprinted with permission from [175], © 2020 Elsevier; (**b**) porosity gradient graphite anode, adapted with permission from [177]; (**c**) 3D CNT/Si core-shell structure, reprinted with permission from [183], Copyright © 2009 American Chemical Society.

Processing technique is key when it comes to microstructure control. In the mass production of composite electrodes, slurring mixing, coating, drying, and calendaring are among the most important steps. Homogeneous distribution of active material from the surface to the bulk of the electrode and microstructure control for optimal porosity, tortuosity, and surface area are achieved by appropriate material selection and manipulation of process knobs such as solvent percentage, drying temperature, compaction pressure, and duration [186]. Novel techniques, including coextrusion, freeze casting, laser patterning, and electric-field or magnetic-field assisted fabrication, have proved effective in reducing electrode tortuosity and improving charging kinetics [175,187–190]. However, challenges such as cost reduction exist before the scaling-up of these approaches.

5. Conclusions and Outlook

Fast charging is currently one of the bottlenecks that limit EV development. Electrode characteristics and electrode engineering are among the most relevant and essential factors of enabling fast charging using Li ion and Li metal batteries.

By reviewing the kinetic processes involved in battery charging, it is found that the intrinsic properties of electrode active materials, as well as the microstructures of electrodes, are both playing a crucial role in determining electrode kinetics. Conduction and mass transport, along with phase transition kinetics, are the three key properties that determine the rate capability of electrode active materials. Microstructures, on the other hand, offer more tunability in electrode properties. For dense structures, grain size and crystallographic orientation should be considered when estimating the effective conductivity and diffusivity. For composite structures, particle size, porosity, and tortuosity are the most important characteristics that govern electrode kinetics. Under some circumstances, e.g., when particles are small enough, the impacts of microstructure can outweigh those of intrinsic material properties.

A major hurdle to fast charging is the degradation of electrodes. When it comes to this topic, it is noteworthy that there are two main categories of fast-charging-related degradation mechanisms. The first category is a direct consequence of the elevated over-potential caused by fast charging, including degradation mechanisms such as Li dendrite growth on anodes and cathode structural instabilities. The second category is composed of degradation mechanisms that exist at all charge rates but are aggravated by the spatial inhomogeneities in Li concentration induced by fast charging. Examples are the growth of unstable SEI and CEI, mechanical degradation, and unfavorable processes related to electrode microstructures.

Given the abovementioned degradation mechanisms, solutions are needed to address the challenges of fast charging both on the material and on the electrode level. Composition optimization serves different purposes for anodes and cathodes. For anodes, the objective is to improve electrode kinetics related to conduction and diffusion. For cathodes, however, the objective is to stabilize the pristine structure during charging. Surface modification and microstructure control are significant to both electrodes, with the top goals being to speed up the kinetics and suppress unfavorable side reactions. Future electrode engineering should focus not only on reducing fast-charging-related overpotentials, but also on alleviating

inhomogeneities in Li concentration, stress distribution, and heat distribution during fast charging, all of which requires an in-depth understanding of kinetic limitations on electrode-related reactions. Other than electrode engineering, attention should also be paid to the optimization of battery electrolytes. Improving Li ion conductivity and the compatibility between electrolyte and electrodes are essential in enabling fast charging in Li-based batteries. Manipulation of co-solvent, salt concentration, and composition, as well as new electrolyte additives are promising paths forwards.

Institutional Review Board Statement: .Not applicable.

Informed Consent Statement: Not applicable.

Data Availability Statement: Not applicable.

Conflicts of Interest: The authors declare no conflict of interest.

References

1. Nishi, Y. Lithium ion secondary batteries; past 10 years and the future. *J. Power Sources* **2001**, *100*, 101–106. [CrossRef]
2. Nitta, N.; Wu, F.; Lee, J.T.; Yushin, G. Li-ion battery materials: Present and future. *Mater. Today* **2015**, *18*, 252–264. [CrossRef]
3. Closing the Gap to Extreme Fast Charge. Available online: https://www.anl.gov/access/research/projects/extreme-fast-charge (accessed on 22 March 2023).
4. Supercharger. Available online: https://www.tesla.com/supercharger (accessed on 22 March 2023).
5. Introducing V3 Supercharging. Available online: https://www.tesla.com/en_GB/blog/introducing-v3-supercharging (accessed on 22 March 2023).
6. Doll, S. Electrify America's First Megawatt-Level Battery Storage-Backed Charging Station Reduces Stress on the Grid. Available online: https://electrek.co/2022/10/19/electrify-america-megawatt-level-battery-storage-charging-station/ (accessed on 22 March 2023).
7. Tian, J.; Li, S.; Liu, X.; Yang, D.; Wang, P.; Chang, G. Lithium-ion battery charging optimization based on electrical, thermal and aging mechanism models. *Energy Rep.* **2022**, *8*, 13723–13734. [CrossRef]
8. Yang, Z.; Charalambous, H.; Lin, Y.; Trask, S.E.; Yu, L.; Wen, J.; Jansen, A.; Tsai, Y.; Wiaderek, K.M.; Ren, Y. Extreme fast charge aging: Correlation between electrode scale and heterogeneous degradation in Ni-rich layered cathodes. *J. Power Sources* **2022**, *521*, 230961. [CrossRef]
9. Tanim, T.R.; Paul, P.P.; Thampy, V.; Cao, C.; Steinrück, H.-G.; Weker, J.N.; Toney, M.F.; Dufek, E.J.; Evans, M.C.; Jansen, A.N. Heterogeneous behavior of lithium plating during extreme fast charging. *Cell Rep. Phys. Sci.* **2020**, *1*, 100114. [CrossRef]
10. Fear, C.; Adhikary, T.; Carter, R.; Mistry, A.N.; Love, C.T.; Mukherjee, P.P. In operando detection of the onset and mapping of lithium plating regimes during fast charging of lithium-ion batteries. *ACS Appl. Mater. Interfaces* **2020**, *12*, 30438–30448. [CrossRef]
11. Anseán, D.; Dubarry, M.; Devie, A.; Liaw, B.; García, V.; Viera, J.; González, M. Fast charging technique for high power LiFePO$_4$ batteries: A mechanistic analysis of aging. *J. Power Sources* **2016**, *321*, 201–209. [CrossRef]
12. Al-Saadi, M.; Olmos, J.; Saez-de-Ibarra, A.; Van Mierlo, J.; Berecibar, M. Fast charging impact on the lithium-ion batteries' lifetime and cost-effective battery sizing in heavy-duty electric vehicles applications. *Energies* **2022**, *15*, 1278. [CrossRef]
13. Li, J.; Dudney, N.J.; Xiao, X.; Cheng, Y.T.; Liang, C.; Verbrugge, M.W. Asymmetric rate behavior of Si anodes for lithium-ion batteries: Ultrafast de-lithiation versus sluggish lithiation at high current densities. *Adv. Energy Mater.* **2015**, *5*, 1401627. [CrossRef]
14. Yang, H.; Wu, H.H.; Ge, M.; Li, L.; Yuan, Y.; Yao, Q.; Chen, J.; Xia, L.; Zheng, J.; Chen, Z. Simultaneously dual modification of Ni-rich layered oxide cathode for high-energy lithium-ion batteries. *Adv. Funct. Mater.* **2019**, *29*, 1808825. [CrossRef]
15. Radin, M.D.; Hy, S.; Sina, M.; Fang, C.; Liu, H.; Vinckeviciute, J.; Zhang, M.; Whittingham, M.S.; Meng, Y.S.; Van der Ven, A. Narrowing the gap between theoretical and practical capacities in Li-ion layered oxide cathode materials. *Adv. Energy Mater.* **2017**, *7*, 1602888. [CrossRef]
16. Hausbrand, R.; Cherkashinin, G.; Ehrenberg, H.; Gröting, M.; Albe, K.; Hess, C.; Jaegermann, W. Fundamental degradation mechanisms of layered oxide Li-ion battery cathode materials: Methodology, insights and novel approaches. *Mater. Sci. Eng. B* **2015**, *192*, 3–25. [CrossRef]
17. Zhang, S.S. Unveiling capacity degradation mechanism of Li-ion battery in fast-charging process. *ChemElectroChem* **2020**, *7*, 555–560. [CrossRef]
18. Xia, S.; Mu, L.; Xu, Z.; Wang, J.; Wei, C.; Liu, L.; Pianetta, P.; Zhao, K.; Yu, X.; Lin, F. Chemomechanical interplay of layered cathode materials undergoing fast charging in lithium batteries. *Nano Energy* **2018**, *53*, 753–762. [CrossRef]
19. Tanim, T.R.; Yang, Z.; Colclasure, A.M.; Chinnam, P.R.; Gasper, P.; Lin, Y.; Yu, L.; Weddle, P.J.; Wen, J.; Dufek, E.J. Extended cycle life implications of fast charging for lithium-ion battery cathode. *Energy Storage Mater.* **2021**, *41*, 656–666. [CrossRef]
20. Son, S.-B.; Robertson, D.; Yang, Z.; Tsai, Y.; Lopykinski, S.; Bloom, I. Fast charge-driven Li plating on anode and structural degradation of cathode. *J. Electrochem. Soc.* **2020**, *167*, 140506. [CrossRef]

21. Colclasure, A.M.; Dunlop, A.R.; Trask, S.E.; Polzin, B.J.; Jansen, A.N.; Smith, K. Requirements for enabling extreme fast charging of high energy density Li-ion cells while avoiding lithium plating. *J. Electrochem. Soc.* **2019**, *166*, A1412. [CrossRef]

22. Liu, Y.; Zhu, Y.; Cui, Y. Challenges and opportunities towards fast-charging battery materials. *Nat. Energy* **2019**, *4*, 540–550. [CrossRef]

23. Keyser, M.; Pesaran, A.; Li, Q.; Santhanagopalan, S.; Smith, K.; Wood, E.; Ahmed, S.; Bloom, I.; Dufek, E.; Shirk, M. Enabling fast charging–Battery thermal considerations. *J. Power Sources* **2017**, *367*, 228–236. [CrossRef]

24. Yao, Y.X.; Chen, X.; Yao, N.; Gao, J.H.; Xu, G.; Ding, J.F.; Song, C.L.; Cai, W.L.; Yan, C.; Zhang, Q. Unlocking Charge Transfer Limitations for Extreme Fast Charging of Li-Ion Batteries. *Angew. Chem. Int. Ed.* **2023**, *62*, e202214828.

25. Ahmed, S.; Bloom, I.; Jansen, A.N.; Tanim, T.; Dufek, E.J.; Pesaran, A.; Burnham, A.; Carlson, R.B.; Dias, F.; Hardy, K. Enabling fast charging–A battery technology gap assessment. *J. Power Sources* **2017**, *367*, 250–262. [CrossRef]

26. Pharr, M.; Zhao, K.; Wang, X.; Suo, Z.; Vlassak, J.J. Kinetics of initial lithiation of crystalline silicon electrodes of lithium-ion batteries. *Nano Lett.* **2012**, *12*, 5039–5047. [CrossRef] [PubMed]

27. Miao, J.; Thompson, C.V. Kinetic study of the initial lithiation of amorphous silicon thin film anodes. *J. Electrochem. Soc.* **2018**, *165*, A650. [CrossRef]

28. Zlatilova, P.; Balkanov, I.; Geronov, Y. Thin foil lithium-aluminium electrode. The effect of thermal treatment on its electrochemical behaviour in nonaqueous media. *J. Power Sources* **1988**, *24*, 71–79. [CrossRef]

29. Geronov, Y.; Zlatilova, P.; Staikov, G. The secondary lithium—Aluminium electrode at room temperature. II. Kinetics of the electrochemical formation of the lithium—Aluminium alloy. *J. Power Sources* **1984**, *12*, 155–165. [CrossRef]

30. Miao, J.; Wang, B.; Thompson, C.V. Kinetic study of lithiation-induced phase transitions in amorphous germanium thin films. *J. Electrochem. Soc.* **2020**, *167*, 090557. [CrossRef]

31. Li, Y.; Cheng, X.; Zhang, Y.; Zhao, K. Recent advance in understanding the electro-chemo-mechanical behavior of lithium-ion batteries by electron microscopy. *Mater. Today Nano* **2019**, *7*, 100040. [CrossRef]

32. Huo, H.; Janek, J.r. Silicon as Emerging Anode in Solid-State Batteries. *ACS Energy Lett.* **2022**, *7*, 4005–4016. [CrossRef]

33. Tomaszewska, A.; Chu, Z.; Feng, X.; O'kane, S.; Liu, X.; Chen, J.; Ji, C.; Endler, E.; Li, R.; Liu, L. Lithium-ion battery fast charging: A review. *ETransportation* **2019**, *1*, 100011. [CrossRef]

34. Wu, M.; Xu, B.; Ouyang, C. Physics of electron and lithium-ion transport in electrode materials for Li-ion batteries. *Chin. Phys. B* **2015**, *25*, 018206. [CrossRef]

35. Koyama, Y.; Arai, H.; Tanaka, I.; Uchimoto, Y.; Ogumi, Z. Defect chemistry in layered $LiMO_2$ (M = Co, Ni, Mn, and $Li_{1/3}Mn_{2/3}$) by first-principles calculations. *Chem. Mater.* **2012**, *24*, 3886–3894. [CrossRef]

36. Gao, Y.; Xiong, K.; Zhang, H.; Zhu, B. Effect of Ru doping on the properties of $LiFePO_4$/C cathode materials for lithium-ion batteries. *ACS Omega* **2021**, *6*, 14122–14129. [CrossRef] [PubMed]

37. Lee, C.H.; Lee, S.U. p-and n-type Doping Effects on the Electrical and Ionic Conductivities of $Li_4Ti_5O_{12}$ Anode Materials. *J. Phys. Chem. C* **2018**, *122*, 15155–15162. [CrossRef]

38. Young, D.; Ransil, A.; Amin, R.; Li, Z.; Chiang, Y.M. Electronic conductivity in the $Li_{4/3}Ti_{5/3}O_4$–$Li_{7/3}Ti_{5/3}O_4$ system and variation with state-of-charge as a Li battery anode. *Adv. Energy Mater.* **2013**, *3*, 1125–1129. [CrossRef]

39. Van der Ven, A.; Bhattacharya, J.; Belak, A.A. Understanding Li diffusion in Li-intercalation compounds. *Acc. Chem. Res.* **2013**, *46*, 1216–1225. [CrossRef] [PubMed]

40. Persson, K.; Sethuraman, V.A.; Hardwick, L.J.; Hinuma, Y.; Meng, Y.S.; Van Der Ven, A.; Srinivasan, V.; Kostecki, R.; Ceder, G. Lithium diffusion in graphitic carbon. *J. Phys. Chem. Lett.* **2010**, *1*, 1176–1180. [CrossRef]

41. Bates, J.; Dudney, N.; Neudecker, B.; Hart, F.; Jun, H.; Hackney, S. Preferred orientation of polycrystalline $LiCoO_2$ films. *J. Electrochem. Soc.* **2000**, *147*, 59. [CrossRef]

42. Electrochemical Behavior and Li Diffusion Study of $LiCoO_2$ Thin Film Electrodes Prepared by PLD. Available online: https://dspace.mit.edu/handle/1721.1/35827 (accessed on 22 March 2023).

43. Prosini, P.P.; Lisi, M.; Zane, D.; Pasquali, M. Determination of the chemical diffusion coefficient of lithium in $LiFePO_4$. *Solid State Ion.* **2002**, *148*, 45–51. [CrossRef]

44. Malik, R.; Burch, D.; Bazant, M.; Ceder, G. Particle size dependence of the ionic diffusivity. *Nano Lett.* **2010**, *10*, 4123–4127. [CrossRef]

45. Van der Ven, A.; Ceder, G. Lithium diffusion mechanisms in layered intercalation compounds. *J. Power Sources* **2001**, *97*, 529–531. [CrossRef]

46. Pan, J.; Zhang, Q.; Li, J.; Beck, M.J.; Xiao, X.; Cheng, Y.-T. Effects of stress on lithium transport in amorphous silicon electrodes for lithium-ion batteries. *Nano Energy* **2015**, *13*, 192–199. [CrossRef]

47. Zhao, J.; Huang, R.; Gao, W.; Zuo, J.M.; Zhang, X.F.; Misture, S.T.; Chen, Y.; Lockard, J.V.; Zhang, B.; Guo, S. An Ion-Exchange Promoted Phase Transition in a Li-Excess Layered Cathode Material for High-Performance Lithium Ion Batteries. *Adv. Energy Mater.* **2015**, *5*, 1401937. [CrossRef]

48. Nam, K.-W.; Yoon, W.-S.; Yang, X.-Q. Structural changes and thermal stability of charged $LiNi_{1/3}Co_{1/3}Mn_{1/3}O_2$ cathode material for Li-ion batteries studied by time-resolved XRD. *J. Power Sources* **2009**, *189*, 515–518. [CrossRef]

49. Hong, J.; Wang, C.; Kasavajjula, U. Kinetic behavior of $LiFeMgPO_4$ cathode material for Li-ion batteries. *J. Power Sources* **2006**, *162*, 1289–1296. [CrossRef]

50. Barai, A.; Uddin, K.; Dubarry, M.; Somerville, L.; McGordon, A.; Jennings, P.; Bloom, I. A comparison of methodologies for the non-invasive characterisation of commercial Li-ion cells. *Prog. Energy Combust. Sci.* **2019**, *72*, 1–31. [CrossRef]

51. Miao, J.; Wang, B.; Thompson, C.V. First-order amorphous-to-amorphous phase transitions during lithiation of silicon thin films. *Phys. Rev. Mater.* **2020**, *4*, 043608. [CrossRef]

52. Meethong, N.; Huang, H.Y.; Speakman, S.A.; Carter, W.C.; Chiang, Y.M. Strain accommodation during phase transformations in olivine-based cathodes as a materials selection criterion for high-power rechargeable batteries. *Adv. Funct. Mater.* **2007**, *17*, 1115–1123. [CrossRef]

53. Rudraraju, S.; Van der Ven, A.; Garikipati, K. Mechanochemical spinodal decomposition: A phenomenological theory of phase transformations in multi-component, crystalline solids. *npj Comput. Mater.* **2016**, *2*, 16012. [CrossRef]

54. Kim, S.; Lee, J. Spinodal decomposition: A new approach to hierarchically porous inorganic materials for energy storage. *Natl. Sci. Rev.* **2020**, *7*, 1635–1637. [CrossRef]

55. Bai, P.; Cogswell, D.A.; Bazant, M.Z. Suppression of phase separation in $LiFePO_4$ nanoparticles during battery discharge. *Nano Lett.* **2011**, *11*, 4890–4896. [CrossRef]

56. Zheng, T.; Kramer, D.; Mönig, R.; Boles, S.T. Aluminum Foil Anodes for Li-Ion Rechargeable Batteries: The Role of Li Solubility within β-LiAl. *ACS Sustain. Chem. Eng.* **2022**, *10*, 3203–3210. [CrossRef]

57. Yamakawa, S.; Yamasaki, H.; Koyama, T.; Asahi, R. Numerical study of Li diffusion in polycrystalline $LiCoO_2$. *J. Power Sources* **2013**, *223*, 199–205. [CrossRef]

58. Park, M.; Zhang, X.; Chung, M.; Less, G.B.; Sastry, A.M. A review of conduction phenomena in Li-ion batteries. *J. Power Sources* **2010**, *195*, 7904–7929. [CrossRef]

59. Zhao, Y.; Peng, L.; Liu, B.; Yu, G. Single-crystalline $LiFePO_4$ nanosheets for high-rate Li-ion batteries. *Nano Lett.* **2014**, *14*, 2849–2853. [CrossRef] [PubMed]

60. Liu, X.; Zheng, B.; Zhao, J.; Zhao, W.; Liang, Z.; Su, Y.; Xie, C.; Zhou, K.; Xiang, Y.; Zhu, J. Electrochemo-mechanical effects on structural integrity of Ni-rich cathodes with different microstructures in all solid-state batteries. *Adv. Energy Mater.* **2021**, *11*, 2003583. [CrossRef]

61. Langdon, J.; Manthiram, A. A perspective on single-crystal layered oxide cathodes for lithium-ion batteries. *Energy Storage Mater.* **2021**, *37*, 143–160. [CrossRef]

62. Han, Y.; Jung, S.H.; Kwak, H.; Jun, S.; Kwak, H.H.; Lee, J.H.; Hong, S.T.; Jung, Y.S. Single-or poly-crystalline ni-rich layered cathode, sulfide or halide solid electrolyte: Which will be the winners for all-solid-state batteries? *Adv. Energy Mater.* **2021**, *11*, 2100126. [CrossRef]

63. Shi, F.; Song, Z.; Ross, P.N.; Somorjai, G.A.; Ritchie, R.O.; Komvopoulos, K. Failure mechanisms of single-crystal silicon electrodes in lithium-ion batteries. *Nat. Commun.* **2016**, *7*, 11886. [CrossRef]

64. Xu, Z.; Jiang, Z.; Kuai, C.; Xu, R.; Qin, C.; Zhang, Y.; Rahman, M.M.; Wei, C.; Nordlund, D.; Sun, C.-J. Charge distribution guided by grain crystallographic orientations in polycrystalline battery materials. *Nat. Commun.* **2020**, *11*, 83. [CrossRef]

65. Wang, R.; Chen, X.; Huang, Z.; Yang, J.; Liu, F.; Chu, M.; Liu, T.; Wang, C.; Zhu, W.; Li, S. Twin boundary defect engineering improves lithium-ion diffusion for fast-charging spinel cathode materials. *Nat. Commun.* **2021**, *12*, 3085. [CrossRef]

66. Bläubaum, L.; Röder, F.; Nowak, C.; Chan, H.S.; Kwade, A.; Krewer, U. Impact of Particle Size Distribution on Performance of Lithium-Ion Batteries. *ChemElectroChem* **2020**, *7*, 4755–4766. [CrossRef]

67. Liu, B.; Xu, J. Cracks of silicon nanoparticles in anodes: Mechanics–electrochemical-coupled modeling framework based on the phase-field method. *ACS Appl. Energy Mater.* **2020**, *3*, 10931–10939. [CrossRef]

68. Strauss, F.; Bartsch, T.; de Biasi, L.; Kim, A.-Y.; Janek, J.r.; Hartmann, P.; Brezesinski, T. Impact of cathode material particle size on the capacity of bulk-type all-solid-state batteries. *ACS Energy Lett.* **2018**, *3*, 992–996. [CrossRef]

69. Chen, D.; He, H.; Zhang, D.; Wang, H.; Ni, M. Percolation theory in solid oxide fuel cell composite electrodes with a mixed electronic and ionic conductor. *Energies* **2013**, *6*, 1632–1656. [CrossRef]

70. Pohjalainen, E.; Rauhala, T.; Valkeapää, M.; Kallioinen, J.; Kallio, T. Effect of $Li_4Ti_5O_{12}$ particle size on the performance of lithium ion battery electrodes at high C-rates and low temperatures. *J. Phys. Chem. C* **2015**, *119*, 2277–2283. [CrossRef]

71. Ito, Y.; Yamakawa, S.; Hayashi, A.; Tatsumisago, M. Effects of the microstructure of solid-electrolyte-coated $LiCoO_2$ on its discharge properties in all-solid-state lithium batteries. *J. Mater. Chem. A* **2017**, *5*, 10658–10668. [CrossRef]

72. Qiu, L.; Zhang, M.; Song, Y.; Wu, Z.; Hu, K.; Yue, L.; Zhang, J.; Ming, Y.; Xiang, W.; Wang, G. The structure-activity relationship between precursor fine structure and cathode performance in ultra-high Ni layered oxide. *Chem. Eng. Sci.* **2022**, *260*, 117865. [CrossRef]

73. Wagner, A.C.; Bohn, N.; Geßwein, H.; Neumann, M.; Osenberg, M.; Hilger, A.; Manke, I.; Schmidt, V.; Binder, J.R. Hierarchical Structuring of NMC111-Cathode Materials in Lithium-Ion Batteries: An In-Depth Study on the Influence of Primary and Secondary Particle Sizes on Electrochemical Performance. *ACS Appl. Energy Mater.* **2020**, *3*, 12565–12574. [CrossRef]

74. Taleghani, S.T.; Marcos, B.; Zaghib, K.; Lantagne, G. A study on the effect of porosity and particles size distribution on Li-ion battery performance. *J. Electrochem. Soc.* **2017**, *164*, E3179. [CrossRef]

75. Vishnugopi, B.S.; Verma, A.; Mukherjee, P.P. Fast charging of lithium-ion batteries via electrode engineering. *J. Electrochem. Soc.* **2020**, *167*, 090508. [CrossRef]

76. Elango, R.; Nadeina, A.; Cadiou, F.; De Andrade, V.; Demortière, A.; Morcrette, M.; Seznec, V. Impact of electrode porosity architecture on electrochemical performances of 1 mm-thick LiFePO$_4$ binder-free Li-ion electrodes fabricated by Spark Plasma Sintering. *J. Power Sources* **2021**, *488*, 229402. [CrossRef]

77. Zhang, S.S.; Xu, K.; Jow, T. Study of the charging process of a LiCoO$_2$-based Li-ion battery. *J. Power Sources* **2006**, *160*, 1349–1354. [CrossRef]

78. Weiss, M.; Ruess, R.; Kasnatscheew, J.; Levartovsky, Y.; Levy, N.R.; Minnmann, P.; Stolz, L.; Waldmann, T.; Wohlfahrt-Mehrens, M.; Aurbach, D. Fast charging of lithium-ion batteries: A review of materials aspects. *Adv. Energy Mater.* **2021**, *11*, 2101126. [CrossRef]

79. Yao, K.P.; Okasinski, J.S.; Kalaga, K.; Shkrob, I.A.; Abraham, D.P. Quantifying lithium concentration gradients in the graphite electrode of Li-ion cells using operando energy dispersive X-ray diffraction. *Energy Environ. Sci.* **2019**, *12*, 656–665. [CrossRef]

80. Finegan, D.P.; Quinn, A.; Wragg, D.S.; Colclasure, A.M.; Lu, X.; Tan, C.; Heenan, T.M.; Jervis, R.; Brett, D.J.; Das, S. Spatial dynamics of lithiation and lithium plating during high-rate operation of graphite electrodes. *Energy Environ. Sci.* **2020**, *13*, 2570–2584. [CrossRef]

81. Colclasure, A.M.; Tanim, T.R.; Jansen, A.N.; Trask, S.E.; Dunlop, A.R.; Polzin, B.J.; Bloom, I.; Robertson, D.; Flores, L.; Evans, M. Electrode scale and electrolyte transport effects on extreme fast charging of lithium-ion cells. *Electrochim. Acta* **2020**, *337*, 135854. [CrossRef]

82. Mistry, A.; Usseglio-Viretta, F.L.; Colclasure, A.; Smith, K.; Mukherjee, P.P. Fingerprinting redox heterogeneity in electrodes during extreme fast charging. *J. Electrochem. Soc.* **2020**, *167*, 090542. [CrossRef]

83. Lin, X.; Khosravinia, K.; Hu, X.; Li, J.; Lu, W. Lithium plating mechanism, detection, and mitigation in lithium-ion batteries. *Prog. Energy Combust. Sci.* **2021**, *87*, 100953. [CrossRef]

84. Han, X.; Meng, Q.; Wan, X.; Sun, B.; Zhang, Y.; Shen, B.; Gao, J.; Ma, Y.; Zuo, P.; Lou, S. Intercalation pseudocapacitive electrochemistry of Nb-based oxides for fast charging of lithium-ion batteries. *Nano Energy* **2021**, *81*, 105635. [CrossRef]

85. Belharouak, I.; Koenig, G.M.; Tan, T.; Yumoto, H.; Ota, N.; Amine, K. Performance degradation and gassing of Li$_4$Ti$_5$O$_{12}$/LiMn$_2$O$_4$ lithium-ion cells. *J. Electrochem. Soc.* **2012**, *159*, A1165. [CrossRef]

86. Deng, Q.; Fu, Y.; Zhu, C.; Yu, Y. Niobium-based oxides toward advanced electrochemical energy storage: Recent advances and challenges. *Small* **2019**, *15*, 1804884. [CrossRef] [PubMed]

87. Gao, T.; Han, Y.; Fraggedakis, D.; Das, S.; Zhou, T.; Yeh, C.-N.; Xu, S.; Chueh, W.C.; Li, J.; Bazant, M.Z. Interplay of lithium intercalation and plating on a single graphite particle. *Joule* **2021**, *5*, 393–414. [CrossRef]

88. Hou, G.; Sun, Q.; Ai, Q.; Ren, X.; Xu, X.; Guo, H.; Guo, S.; Zhang, L.; Feng, J.; Ding, F. Growth direction control of lithium dendrites in a heterogeneous lithiophilic host for ultra-safe lithium metal batteries. *J. Power Sources* **2019**, *416*, 141–147. [CrossRef]

89. He, Y.; Ren, X.; Xu, Y.; Engelhard, M.H.; Li, X.; Xiao, J.; Liu, J.; Zhang, J.-G.; Xu, W.; Wang, C. Origin of lithium whisker formation and growth under stress. *Nat. Nanotechnol.* **2019**, *14*, 1042–1047. [CrossRef]

90. Rangarajan, S.P.; Barsukov, Y.; Mukherjee, P.P. In operando signature and quantification of lithium plating. *J. Mater. Chem. A* **2019**, *7*, 20683–20695. [CrossRef]

91. Ling, C.; Banerjee, D.; Matsui, M. Study of the electrochemical deposition of Mg in the atomic level: Why it prefers the non-dendritic morphology. *Electrochim. Acta* **2012**, *76*, 270–274. [CrossRef]

92. Wasalathanthri, R.N.; Akolkar, R. Perspective—Does the Sand Equation Reliably Predict the Onset of Morphological Evolution in Lithium Electrodeposition? *J. Electrochem. Soc.* **2022**, *169*, 092519. [CrossRef]

93. Shen, L.; Shi, P.; Hao, X.; Zhao, Q.; Ma, J.; He, Y.B.; Kang, F. Progress on lithium dendrite suppression strategies from the interior to exterior by hierarchical structure designs. *Small* **2020**, *16*, 2000699. [CrossRef]

94. Jang, T.; Kang, J.-H.; Kim, S.; Shim, M.; Lee, J.; Song, J.; Kim, W.; Ryu, K.; Byon, H.R. Nanometer-Scale Surface Roughness of a 3-D Cu Substrate Promoting Li Nucleation in Li-Metal Batteries. *ACS Appl. Energy Mater.* **2021**, *4*, 2644–2651. [CrossRef]

95. Gallagher, K.G.; Trask, S.E.; Bauer, C.; Woehrle, T.; Lux, S.F.; Tschech, M.; Lamp, P.; Polzin, B.J.; Ha, S.; Long, B. Optimizing areal capacities through understanding the limitations of lithium-ion electrodes. *J. Electrochem. Soc.* **2015**, *163*, A138. [CrossRef]

96. Zhu, Y.; Xie, J.; Pei, A.; Liu, B.; Wu, Y.; Lin, D.; Li, J.; Wang, H.; Chen, H.; Xu, J. Fast lithium growth and short circuit induced by localized-temperature hotspots in lithium batteries. *Nat. Commun.* **2019**, *10*, 2067. [CrossRef] [PubMed]

97. Wang, X.; Zeng, W.; Hong, L.; Xu, W.; Yang, H.; Wang, F.; Duan, H.; Tang, M.; Jiang, H. Stress-driven lithium dendrite growth mechanism and dendrite mitigation by electroplating on soft substrates. *Nat. Energy* **2018**, *3*, 227–235. [CrossRef]

98. Edge, J.S.; O'Kane, S.; Prosser, R.; Kirkaldy, N.D.; Patel, A.N.; Hales, A.; Ghosh, A.; Ai, W.; Chen, J.; Yang, J. Lithium ion battery degradation: What you need to know. *Phys. Chem. Chem. Phys.* **2021**, *23*, 8200–8221. [CrossRef] [PubMed]

99. Cheng, E.J.; Sharafi, A.; Sakamoto, J. Intergranular Li metal propagation through polycrystalline Li$_{6.25}$Al$_{0.25}$La$_3$Zr$_2$O$_{12}$ ceramic electrolyte. *Electrochim. Acta* **2017**, *223*, 85–91. [CrossRef]

100. Rangarajan, S.P.; Barsukov, Y.; Mukherjee, P.P. Plating energy as a universal descriptor to classify accelerated cell failure under operational extremes. *Cell Rep. Phys. Sci.* **2022**, *3*, 100720. [CrossRef]

101. Nie, M.; Abraham, D.P.; Chen, Y.; Bose, A.; Lucht, B.L. Silicon solid electrolyte interphase (SEI) of lithium ion battery characterized by microscopy and spectroscopy. *J. Phys. Chem. C* **2013**, *117*, 13403–13412. [CrossRef]

102. Fong, R.; Von Sacken, U.; Dahn, J.R. Studies of lithium intercalation into carbons using nonaqueous electrochemical cells. *J. Electrochem. Soc.* **1990**, *137*, 2009. [CrossRef]

103. Narayanan, S.; Ulissi, U.; Gibson, J.S.; Chart, Y.A.; Weatherup, R.S.; Pasta, M. Effect of current density on the solid electrolyte interphase formation at the lithium| Li$_6$PS$_5$Cl interface. *Nat. Commun.* **2022**, *13*, 7237. [CrossRef]

104. Yoon, T.; Milien, M.S.; Parimalam, B.S.; Lucht, B.L. Thermal decomposition of the solid electrolyte interphase (SEI) on silicon electrodes for lithium ion batteries. *Chem. Mater.* **2017**, *29*, 3237–3245. [CrossRef]
105. Ding, J.-F.; Xu, R.; Yan, C.; Li, B.-Q.; Yuan, H.; Huang, J.-Q. A review on the failure and regulation of solid electrolyte interphase in lithium batteries. *J. Energy Chem.* **2021**, *59*, 306–319. [CrossRef]
106. He, Y.; Jiang, L.; Chen, T.; Xu, Y.; Jia, H.; Yi, R.; Xue, D.; Song, M.; Genc, A.; Bouchet-Marquis, C. Progressive growth of the solid–electrolyte interphase towards the Si anode interior causes capacity fading. *Nat. Nanotechnol.* **2021**, *16*, 1113–1120. [CrossRef] [PubMed]
107. Cheng, X.B.; Zhang, R.; Zhao, C.Z.; Wei, F.; Zhang, J.G.; Zhang, Q. A review of solid electrolyte interphases on lithium metal anode. *Adv. Sci.* **2016**, *3*, 1500213. [CrossRef] [PubMed]
108. Kang, C.S.; Son, S.-B.; Kim, J.W.; Kim, S.C.; Choi, Y.S.; Heo, J.Y.; Suh, S.-S.; Kim, Y.-U.; Chu, Y.Y.; Cho, J.S. Electrochemically induced and orientation dependent crack propagation in single crystal silicon. *J. Power Sources* **2014**, *267*, 739–743. [CrossRef]
109. Li, J.; Dozier, A.K.; Li, Y.; Yang, F.; Cheng, Y.-T. Crack pattern formation in thin film lithium-ion battery electrodes. *J. Electrochem. Soc.* **2011**, *158*, A689. [CrossRef]
110. Wang, J.W.; He, Y.; Fan, F.; Liu, X.H.; Xia, S.; Liu, Y.; Harris, C.T.; Li, H.; Huang, J.Y.; Mao, S.X. Two-phase electrochemical lithiation in amorphous silicon. *Nano Lett.* **2013**, *13*, 709–715. [CrossRef]
111. McDowell, M.T.; Lee, S.W.; Harris, J.T.; Korgel, B.A.; Wang, C.; Nix, W.D.; Cui, Y. In situ TEM of two-phase lithiation of amorphous silicon nanospheres. *Nano Lett.* **2013**, *13*, 758–764. [CrossRef]
112. Liu, X.H.; Zhong, L.; Huang, S.; Mao, S.X.; Zhu, T.; Huang, J.Y. Size-dependent fracture of silicon nanoparticles during lithiation. *ACS Nano* **2012**, *6*, 1522–1531. [CrossRef]
113. Ryu, I.; Choi, J.W.; Cui, Y.; Nix, W.D. Size-dependent fracture of Si nanowire battery anodes. *J. Mech. Phys. Solids* **2011**, *59*, 1717–1730. [CrossRef]
114. Ma, Z.; Li, T.; Huang, Y.; Liu, J.; Zhou, Y.; Xue, D. Critical silicon-anode size for averting lithiation-induced mechanical failure of lithium-ion batteries. *RSC Adv.* **2013**, *3*, 7398–7402. [CrossRef]
115. Barai, P.; Huang, B.; Dillon, S.J.; Mukherjee, P.P. Mechano-electrochemical interaction gives rise to strain relaxation in Sn electrodes. *J. Electrochem. Soc.* **2016**, *163*, A3022. [CrossRef]
116. Key, B.; Bhattacharyya, R.; Morcrette, M.; Seznec, V.; Tarascon, J.-M.; Grey, C.P. Real-time NMR investigations of structural changes in silicon electrodes for lithium-ion batteries. *J. Am. Chem. Soc.* **2009**, *131*, 9239–9249. [CrossRef]
117. Jung, H.; Allan, P.K.; Hu, Y.-Y.; Borkiewicz, O.J.; Wang, X.-L.; Han, W.-Q.; Du, L.-S.; Pickard, C.J.; Chupas, P.J.; Chapman, K.W. Elucidation of the local and long-range structural changes that occur in germanium anodes in lithium-ion batteries. *Chem. Mater.* **2015**, *27*, 1031–1041. [CrossRef]
118. Key, B.; Morcrette, M.; Tarascon, J.-M.; Grey, C.P. Pair distribution function analysis and solid state NMR studies of silicon electrodes for lithium ion batteries: Understanding the (de) lithiation mechanisms. *J. Am. Chem. Soc.* **2011**, *133*, 503–512. [CrossRef] [PubMed]
119. Trill, J.-H.; Tao, C.; Winter, M.; Passerini, S.; Eckert, H. NMR investigations on the lithiation and delithiation of nanosilicon-based anodes for Li-ion batteries. *J. Solid State Electrochem.* **2011**, *15*, 349–356. [CrossRef]
120. Ogata, K.; Salager, E.; Kerr, C.; Fraser, A.; Ducati, C.; Morris, A.J.; Hofmann, S.; Grey, C.P. Revealing lithium–silicide phase transformations in nano-structured silicon-based lithium ion batteries via in situ NMR spectroscopy. *Nat. Commun.* **2014**, *5*, 3217. [CrossRef] [PubMed]
121. Tang, W.; Liu, Y.; Peng, C.; Hu, M.Y.; Deng, X.; Lin, M.; Hu, J.Z.; Loh, K.P. Probing lithium germanide phase evolution and structural change in a germanium-in-carbon nanotube energy storage system. *J. Am. Chem. Soc.* **2015**, *137*, 2600–2607. [CrossRef] [PubMed]
122. Wang, L.; Qiu, J.; Wang, X.; Chen, L.; Cao, G.; Wang, J.; Zhang, H.; He, X. Insights for understanding multiscale degradation of LiFePO$_4$ cathodes. *EScience* **2022**, *2*, 125–137. [CrossRef]
123. Chinnam, P.R.; Colclasure, A.M.; Chen, B.-R.; Tanim, T.R.; Dufek, E.J.; Smith, K.; Evans, M.C.; Dunlop, A.R.; Trask, S.E.; Polzin, B.J. Fast-charging aging considerations: Incorporation and alignment of cell design and material degradation pathways. *ACS Appl. Energy Mater.* **2021**, *4*, 9133–9143. [CrossRef]
124. Daniel, C.; Mohanty, D.; Li, J.; Wood, D.L. Cathode materials review. In *AIP Conference Proceedings*; American Institute of Physics: College Park, MD, USA, 2014; pp. 26–43.
125. Kasnatscheew, J.; Evertz, M.; Kloepsch, R.; Streipert, B.; Wagner, R.; Cekic Laskovic, I.; Winter, M. Learning from Electrochemical Data: Simple Evaluation and Classification of LiMO$_2$-type-based Positive Electrodes for Li-Ion Batteries. *Energy Technol.* **2017**, *5*, 1670–1679. [CrossRef]
126. Li, J.; Lin, C.; Weng, M.; Qiu, Y.; Chen, P.; Yang, K.; Huang, W.; Hong, Y.; Li, J.; Zhang, M. Structural origin of the high-voltage instability of lithium cobalt oxide. *Nat. Nanotechnol.* **2021**, *16*, 599–605. [CrossRef]
127. Wang, H.; Jang, Y.I.; Huang, B.; Sadoway, D.R.; Chiang, Y.M. TEM study of electrochemical cycling-induced damage and disorder in LiCoO$_2$ cathodes for rechargeable lithium batteries. *J. Electrochem. Soc.* **1999**, *146*, 473. [CrossRef]
128. Aurbach, D.; Markovsky, B.; Rodkin, A.; Levi, E.; Cohen, Y.; Kim, H.-J.; Schmidt, M. On the capacity fading of LiCoO$_2$ intercalation electrodes:: The effect of cycling, storage, temperature, and surface film forming additives. *Electrochim. Acta* **2002**, *47*, 4291–4306. [CrossRef]

129. Reducing Reliance on Cobalt for Lithium-ion Batteries. Available online: https://www.energy.gov/eere/vehicles/articles/reducing-reliance-cobalt-lithium-ion-batteries (accessed on 22 March 2023).

130. Zheng, J.; Ye, Y.; Liu, T.; Xiao, Y.; Wang, C.; Wang, F.; Pan, F. Ni/Li disordering in layered transition metal oxide: Electrochemical impact, origin, and control. *Acc. Chem. Res.* **2019**, *52*, 2201–2209. [CrossRef]

131. Reed, J.; Ceder, G. Role of electronic structure in the susceptibility of metastable transition-metal oxide structures to transformation. *Chem. Rev.* **2004**, *104*, 4513–4534. [CrossRef]

132. Bak, S.-M.; Hu, E.; Zhou, Y.; Yu, X.; Senanayake, S.D.; Cho, S.-J.; Kim, K.-B.; Chung, K.Y.; Yang, X.-Q.; Nam, K.-W. Structural changes and thermal stability of charged $LiNi_xMn_yCo_zO_2$ cathode materials studied by combined in situ time-resolved XRD and mass spectroscopy. *ACS Appl. Mater. Interfaces* **2014**, *6*, 22594–22601. [CrossRef]

133. Myung, S.-T.; Maglia, F.; Park, K.-J.; Yoon, C.S.; Lamp, P.; Kim, S.-J.; Sun, Y.-K. Nickel-rich layered cathode materials for automotive lithium-ion batteries: Achievements and perspectives. *ACS Energy Lett.* **2017**, *2*, 196–223. [CrossRef]

134. Mijung, N.; Lee, Y.; Cho, J. Water adsorption and storage characteristics of optimized $LiCoO_2$ and $LiNi_{1/3}Co_{1/3}Mn_{1/3}O_2$ composite cathode material for Li-ion cells. *J. Electrochem. Soc.* **2006**, *153*, A935. [CrossRef]

135. Abraham, D.; Twesten, R.; Balasubramanian, M.; Petrov, I.; McBreen, J.; Amine, K. Surface changes on $LiNi_{0.8}Co_{0.2}O_2$ particles during testing of high-power lithium-ion cells. *Electrochem. Commun.* **2002**, *4*, 620–625. [CrossRef]

136. Wang, B.; Zhang, F.-l.; Zhou, X.-a.; Wang, P.; Wang, J.; Ding, H.; Dong, H.; Liang, W.-b.; Zhang, N.-s.; Li, S.-y. Which of the nickel-rich NCM and NCA is structurally superior as a cathode material for lithium-ion batteries? *J. Mater. Chem. A* **2021**, *9*, 13540–13551. [CrossRef]

137. Bloom, I.; Jones, S.A.; Battaglia, V.S.; Henriksen, G.L.; Christophersen, J.P.; Wright, R.B.; Ho, C.D.; Belt, J.R.; Motloch, C.G. Effect of cathode composition on capacity fade, impedance rise and power fade in high-power, lithium-ion cells. *J. Power Sources* **2003**, *124*, 538–550. [CrossRef]

138. Noh, H.-J.; Youn, S.; Yoon, C.S.; Sun, Y.-K. Comparison of the structural and electrochemical properties of layered Li $[Ni_xCo_yMn_z]O_2$ (x= 1/3, 0.5, 0.6, 0.7, 0.8 and 0.85) cathode material for lithium-ion batteries. *J. Power Sources* **2013**, *233*, 121–130. [CrossRef]

139. Julien, C.M.; Mauger, A.; Zaghib, K.; Groult, H. Comparative issues of cathode materials for Li-ion batteries. *Inorganics* **2014**, *2*, 132–154. [CrossRef]

140. Alikin, D.; Slautin, B.; Kholkin, A. Revealing Lithiation Kinetics and Battery Degradation Pathway in $LiMn_2O_4$-Based Commercial Cathodes via Electrochemical Strain Microscopy. *Batteries* **2022**, *8*, 220. [CrossRef]

141. Luo, F.; Wei, C.; Zhang, C.; Gao, H.; Niu, J.; Ma, W.; Peng, Z.; Bai, Y.; Zhang, Z. Operando X-ray diffraction analysis of the degradation mechanisms of a spinel $LiMn_2O_4$ cathode in different voltage windows. *J. Energy Chem.* **2020**, *44*, 138–146. [CrossRef]

142. Sun, S.; Guan, T.; Cheng, X.; Zuo, P.; Gao, Y.; Du, C.; Yin, G. Accelerated aging and degradation mechanism of $LiFePO_4$/graphite batteries cycled at high discharge rates. *RSC Adv.* **2018**, *8*, 25695–25703. [CrossRef] [PubMed]

143. Zhang, W.-J. Structure and performance of $LiFePO_4$ cathode materials: A review. *J. Power Sources* **2011**, *196*, 2962–2970. [CrossRef]

144. Kassem, M.; Delacourt, C. Postmortem analysis of calendar-aged graphite/$LiFePO_4$ cells. *J. Power Sources* **2013**, *235*, 159–171. [CrossRef]

145. Woodford, W.H.; Carter, W.C.; Chiang, Y.-M. Strategies to avert electrochemical shock and their demonstration in spinels. *J. Electrochem. Soc.* **2014**, *161*, F3005. [CrossRef]

146. Woodford, W.H.; Chiang, Y.-M.; Carter, W.C. Electrochemical shock in ion-intercalation materials with limited solid-solubility. *J. Electrochem. Soc.* **2013**, *160*, A1286. [CrossRef]

147. Xu, R.; Sun, H.; de Vasconcelos, L.S.; Zhao, K. Mechanical and structural degradation of $LiNi_xMn_yCo_zO_2$ cathode in Li-ion batteries: An experimental study. *J. Electrochem. Soc.* **2017**, *164*, A3333. [CrossRef]

148. Stenina, I.; Minakova, P.; Kulova, T.; Yaroslavtsev, A. Electrochemical Properties of $LiFePO_4$ Cathodes: The Effect of Carbon Additives. *Batteries* **2022**, *8*, 111. [CrossRef]

149. Ngo, D.T.; Scipioni, R.; Simonsen, S.B.; Jørgensen, P.S.; Jensen, S.H. A TEM study of morphological and structural degradation phenomena in $LiFePO_4$-CB cathodes. *Int. J. Energy Res.* **2016**, *40*, 2022–2032. [CrossRef]

150. Jiang, Z.; Li, J.; Yang, Y.; Mu, L.; Wei, C.; Yu, X.; Pianetta, P.; Zhao, K.; Cloetens, P.; Lin, F. Machine-learning-revealed statistics of the particle-carbon/binder detachment in lithium-ion battery cathodes. *Nat. Commun.* **2020**, *11*, 2310. [CrossRef] [PubMed]

151. Zhang, S.S. Challenges and strategies for fast charge of Li-ion batteries. *ChemElectroChem* **2020**, *7*, 3569–3577. [CrossRef]

152. Han, X.; Zhang, Z.; Chen, H.; Luo, L.; Zhang, Q.; Chen, J.; Chen, S.; Yang, Y. Bulk boron doping and surface carbon coating enabling fast-charging and stable Si anodes: From thin film to thick Si electrodes. *J. Mater. Chem. A* **2021**, *9*, 3628–3636. [CrossRef]

153. Ali, B.; Muhammad, R.; Anang, D.A.; Cho, M.-k.; Kim, J.-Y.; Nam, K.-W. Ge-doped $Li_4Ti_{5-x}Ge_xO_{12}$ (x= 0.05) as a fast-charging, long-life bi-functional anode material for lithium-and sodium-ion batteries. *Ceram. Int.* **2020**, *46*, 16556–16563. [CrossRef]

154. Kim, N.; Chae, S.; Ma, J.; Ko, M.; Cho, J. Fast-charging high-energy lithium-ion batteries via implantation of amorphous silicon nanolayer in edge-plane activated graphite anodes. *Nat. Commun.* **2017**, *8*, 812. [CrossRef]

155. Liu, X.; Xu, G.-L.; Yin, L.; Hwang, I.; Li, Y.; Lu, L.; Xu, W.; Zhang, X.; Chen, Y.; Ren, Y. Probing the thermal-driven structural and chemical degradation of Ni-rich layered cathodes by Co/Mn exchange. *J. Am. Chem. Soc.* **2020**, *142*, 19745–19753. [CrossRef]

156. Yuge, R.; Tamura, N.; Manako, T.; Nakano, K.; Nakahara, K. High-rate charge/discharge properties of Li-ion battery using carbon-coated composites of graphites, vapor grown carbon fibers, and carbon nanohorns. *J. Power Sources* **2014**, *266*, 471–474. [CrossRef]

157. Gohier, A.; Laïk, B.; Kim, K.H.; Maurice, J.L.; Pereira-Ramos, J.P.; Cojocaru, C.S.; Van, P.T. High-Rate Capability Silicon Decorated Vertically Aligned Carbon Nanotubes for Li-Ion Batteries. *Adv. Mater.* **2012**, *24*, 2592–2597. [CrossRef]

158. Daigle, J.-C.; Asakawa, Y.; Beaupré, M.; Gariépy, V.; Vieillette, R.; Laul, D.; Trudeau, M.; Zaghib, K. Boosting Ultra-Fast Charge Battery Performance: Filling Porous nanoLi$_4$Ti$_5$O$_{12}$ Particles with 3D Network of N-doped Carbons. *Sci. Rep.* **2019**, *9*, 16871. [CrossRef] [PubMed]

159. Kovalenko, I.; Zdyrko, B.; Magasinski, A.; Hertzberg, B.; Milicev, Z.; Burtovyy, R.; Luzinov, I.; Yushin, G. A major constituent of brown algae for use in high-capacity Li-ion batteries. *Science* **2011**, *334*, 75–79. [CrossRef]

160. Shi, Y.; Zhou, X.; Yu, G. Material and structural design of novel binder systems for high-energy, high-power lithium-ion batteries. *Acc. Chem. Res.* **2017**, *50*, 2642–2652. [CrossRef] [PubMed]

161. Xu, T.; Gao, P.; Li, P.; Xia, K.; Han, N.; Deng, J.; Li, Y.; Lu, J. Fast-Charging and Ultrahigh-Capacity Lithium Metal Anode Enabled by Surface Alloying. *Adv. Energy Mater.* **2020**, *10*, 1902343. [CrossRef]

162. Li, N.W.; Yin, Y.X.; Yang, C.P.; Guo, Y.G. An artificial solid electrolyte interphase layer for stable lithium metal anodes. *Adv. Mater.* **2016**, *28*, 1853–1858. [CrossRef]

163. Ho, V.-C.; An, H.; Hong, M.; Lee, S.; Kim, J.; Park, M.B.; Mun, J. A Low Temperature Self-Assembled ZrO$_2$ Layer as a Surface Modification for High Energy Density Ni-Rich Cathode Materials in a Lithium-Ion Battery. *Energy Technol.* **2021**, *9*, 2000800. [CrossRef]

164. Kim, J.Y.; Kim, A.-Y.; Liu, G.; Woo, J.-Y.; Kim, H.; Lee, J.K. Li$_4$SiO$_4$-based artificial passivation thin film for improving interfacial stability of Li metal anodes. *ACS Appl. Mater. Interfaces* **2018**, *10*, 8692–8701. [CrossRef]

165. Li, J.; Dudney, N.J.; Nanda, J.; Liang, C. Artificial solid electrolyte interphase to address the electrochemical degradation of silicon electrodes. *ACS Appl. Mater. Interfaces* **2014**, *6*, 10083–10088. [CrossRef]

166. Al-Obeidi, A.; Kramer, D.; Boles, S.T.; Mönig, R.; Thompson, C.V. Mechanical measurements on lithium phosphorous oxynitride coated silicon thin film electrodes for lithium-ion batteries during lithiation and delithiation. *Appl. Phys. Lett.* **2016**, *109*, 071902. [CrossRef]

167. Yan, S.; Chen, X.; Zhou, P.; Wang, P.; Zhou, H.; Zhang, W.; Xia, Y.; Liu, K. Regulating the growth of lithium dendrite by coating an ultra-thin layer of gold on separator for improving the fast-charging ability of graphite anode. *J. Energy Chem.* **2022**, *67*, 467–473. [CrossRef]

168. Liang, Y.; Chen, Y.; Ke, X.; Zhang, Z.; Wu, W.; Lin, G.; Zhou, Z.; Shi, Z. Coupling of triporosity and strong Au–Li interaction to enable dendrite-free lithium plating/stripping for long-life lithium metal anodes. *J. Mater. Chem. A* **2020**, *8*, 18094–18105. [CrossRef]

169. Zhang, H.; Liao, X.; Guan, Y.; Xiang, Y.; Li, M.; Zhang, W.; Zhu, X.; Ming, H.; Lu, L.; Qiu, J. Lithiophilic-lithiophobic gradient interfacial layer for a highly stable lithium metal anode. *Nat. Commun.* **2018**, *9*, 3729. [CrossRef]

170. He, Y.; Zhang, M.; Wang, A.; Zhang, B.; Pham, H.; Hu, Q.; Sheng, L.; Xu, H.; Wang, L.; Park, J. Regulation of Dendrite-Free Li Plating via Lithiophilic Sites on Lithium-Alloy Surface. *ACS Appl. Mater. Interfaces* **2022**, *14*, 33952–33959. [CrossRef]

171. Zhao, B.; Ma, W.; Li, B.; Hu, X.; Lu, S.; Liu, X.; Jiang, Y.; Zhang, J. A fast and low-cost interface modification method to achieve high-performance garnet-based solid-state lithium metal batteries. *Nano Energy* **2022**, *91*, 106643. [CrossRef]

172. Jiang, W.; Dong, L.; Liu, S.; Ai, B.; Zhao, S.; Zhang, W.; Pan, K.; Zhang, L. Improvement of the interface between the lithium anode and a garnet-type solid electrolyte of lithium batteries using an aluminum-nitride layer. *Nanomaterials* **2022**, *12*, 2023. [CrossRef] [PubMed]

173. Cheng, Q.; Yuge, R.; Nakahara, K.; Tamura, N.; Miyamoto, S. KOH etched graphite for fast chargeable lithium-ion batteries. *J. Power Sources* **2015**, *284*, 258–263. [CrossRef]

174. Huang, Q.; Ni, S.; Jiao, M.; Zhong, X.; Zhou, G.; Cheng, H.M. Aligned Carbon-Based Electrodes for Fast-Charging Batteries: A Review. *Small* **2021**, *17*, 2007676. [CrossRef]

175. Chen, K.-H.; Namkoong, M.J.; Goel, V.; Yang, C.; Kazemiabnavi, S.; Mortuza, S.; Kazyak, E.; Mazumder, J.; Thornton, K.; Sakamoto, J. Efficient fast-charging of lithium-ion batteries enabled by laser-patterned three-dimensional graphite anode architectures. *J. Power Sources* **2020**, *471*, 228475. [CrossRef]

176. Zhao, Z.; Sun, M.; Chen, W.; Liu, Y.; Zhang, L.; Dongfang, N.; Ruan, Y.; Zhang, J.; Wang, P.; Dong, L. Sandwich, vertical-channeled thick electrodes with high rate and cycle performance. *Adv. Funct. Mater.* **2019**, *29*, 1809196. [CrossRef]

177. Yang, J.; Li, Y.; Mijailovic, A.; Wang, G.; Xiong, J.; Mathew, K.; Lu, W.; Sheldon, B.W.; Wu, Q. Gradient porosity electrodes for fast charging lithium-ion batteries. *J. Mater. Chem. A* **2022**, *10*, 12114–12124. [CrossRef]

178. Xu, Y.; Zheng, H.; Yang, H.; Yu, Y.; Luo, J.; Li, T.; Li, W.; Zhang, Y.-N.; Kang, Y. Thermodynamic regulation of dendrite-free Li plating on Li$_3$Bi for stable lithium metal batteries. *Nano Lett.* **2021**, *21*, 8664–8670. [CrossRef] [PubMed]

179. Zhou, G.; Li, H.; Sun, H.; Yu, D.; Wang, Y.; Huang, X.; Chen, L.; Zhang, Z. Controlled Li doping of Si nanowires by electrochemical insertion method. *Appl. Phys. Lett.* **1999**, *75*, 2447–2449. [CrossRef]

180. Park, M.H.; Cho, Y.; Kim, K.; Kim, J.; Liu, M.; Cho, J. Germanium nanotubes prepared by using the kirkendall effect as anodes for high-rate lithium batteries. *Angew. Chem. Int. Ed.* **2011**, *50*, 9647–9650. [CrossRef] [PubMed]

181. Wang, L.; Bao, K.; Lou, Z.; Liang, G.; Zhou, Q. Chemical synthesis of germanium nanoparticles with uniform size as anode materials for lithium ion batteries. *Dalton Trans.* **2016**, *45*, 2814–2817. [CrossRef]

182. Liang, J.; Li, X.; Hou, Z.; Zhang, T.; Zhu, Y.; Yan, X.; Qian, Y. Honeycomb-like macro-germanium as high-capacity anodes for lithium-ion batteries with good cycling and rate performance. *Chem. Mater.* **2015**, *27*, 4156–4164. [CrossRef]

183. Cui, L.-F.; Yang, Y.; Hsu, C.-M.; Cui, Y. Carbon−silicon core−shell nanowires as high capacity electrode for lithium ion batteries. *Nano Lett.* **2009**, *9*, 3370–3374. [CrossRef]

184. Li, H.; Chen, Z.; Kang, Z.; Liu, W.; Chen, Y. High-density crack-resistant Si-C microparticles for lithium ion batteries. *Energy Storage Mater.* **2023**, *56*, 40–49. [CrossRef]

185. Zhang, Q.; Liu, J.; Wu, Z.-Y.; Li, J.-T.; Huang, L.; Sun, S.-G. 3D nanostructured multilayer Si/Al film with excellent cycle performance as anode material for lithium-ion battery. *J. Alloys Compd.* **2016**, *657*, 559–564. [CrossRef]

186. Hawley, W.B.; Li, J. Electrode manufacturing for lithium-ion batteries—Analysis of current and next generation processing. *J. Energy Storage* **2019**, *25*, 100862. [CrossRef]

187. Li, J.; Liang, X.; Liou, F.; Park, J. Macro-/micro-controlled 3D lithium-ion batteries via additive manufacturing and electric field processing. *Sci. Rep.* **2018**, *8*, 1846. [CrossRef]

188. Li, L.; Erb, R.M.; Wang, J.; Wang, J.; Chiang, Y.M. Fabrication of Low-Tortuosity Ultrahigh-Area-Capacity Battery Electrodes through Magnetic Alignment of Emulsion-Based Slurries. *Adv. Energy Mater.* **2019**, *9*, 1802472. [CrossRef]

189. Thakur, A.; Dong, X. Additive manufacturing of 3D structural battery composites with coextrusion deposition of continuous carbon fibers. *Manuf. Lett.* **2020**, *26*, 42–47. [CrossRef]

190. Guo, Y.; Jiang, Y.; Zhang, Q.; Wan, D.; Huang, C. Directional $LiFePO_4$ cathode structure by freeze tape casting to improve lithium ion diffusion kinetics. *J. Power Sources* **2021**, *506*, 230052. [CrossRef]